

# Classifying the $\mathcal{CP}$ properties of the $ggH$ coupling in $H + 2j$ production

Henning Bahl<sup>\*1</sup>, Elina Fuchs<sup>†2,3,4</sup>, Marc Hannig<sup>‡3</sup>, and Marco Menen<sup>§3,4</sup>

<sup>1</sup>*University of Chicago, Department of Physics, 5720 South Ellis Avenue, Chicago, IL 60637 USA*

<sup>2</sup>*CERN, Department of Theoretical Physics, 1211 Geneve 23, Switzerland*

<sup>3</sup>*Institut für Theoretische Physik, Leibniz Universität Hannover, Appelstraße 2, 30167 Hannover, Germany*

<sup>4</sup>*Physikalisch-Technische Bundesanstalt, Bundesallee 100, 38116 Braunschweig, Germany*

September 7, 2023

## Abstract

The Higgs–gluon interaction is crucial for LHC phenomenology. To improve the constraints on the  $\mathcal{CP}$  structure of this coupling, we investigate Higgs production with two jets using machine learning. In particular, we exploit the  $\mathcal{CP}$  sensitivity of the so far neglected phase space region that differs from the typical vector boson fusion-like kinematics. Our results suggest that significant improvements in current experimental limits are possible. We also discuss the most relevant observables and how  $\mathcal{CP}$  violation in the Higgs–gluon interaction can be disentangled from  $\mathcal{CP}$  violation in the interaction between the Higgs boson and massive vector bosons. Assuming the absence of  $\mathcal{CP}$ -violating Higgs interactions with coloured beyond-the-Standard-Model states, our projected limits on a  $\mathcal{CP}$ -violating top-Yukawa coupling are stronger than more direct probes like top-associated Higgs production and limits from a global fit.

---

\*hbahl@uchicago.edu

†elina.fuchs@cern.ch

‡marc.hannig@stud.uni-hannover.de

§marco.menen@itp.uni-hannover.de

# Contents

<b>1</b>	<b>Introduction</b>	<b>3</b>
<b>2</b>	<b>Gluon fusion with two jets in an EFT approach</b>	<b>5</b>
2.1	Gluon fusion in association with two jets . . . . .	5
2.2	Effective Higgs-vector boson interactions . . . . .	6
<b>3</b>	<b>Event generation</b>	<b>7</b>
<b>4</b>	<b>Analysis strategy</b>	<b>10</b>
4.1	Signal-background separation . . . . .	11
4.2	Separating the different ggF2j contributions . . . . .	12
<b>5</b>	<b>Sensitivity to the Higgs–gluon coupling</b>	<b>15</b>
5.1	ggF2j signal region . . . . .	15
5.2	VBF signal region . . . . .	15
5.3	Combination . . . . .	18
5.4	Highest-impact observables . . . . .	20
<b>6</b>	<b>Disentangling <math>\mathcal{CP}</math> violation in the <math>ggH</math> and <math>HVV</math> couplings</b>	<b>22</b>
<b>7</b>	<b>Limits on the <math>\mathcal{CP}</math> structure of the top-Yukawa coupling</b>	<b>24</b>
<b>8</b>	<b>Conclusions</b>	<b>26</b>
<b>A</b>	<b>Details of the event generation</b>	<b>27</b>
<b>B</b>	<b>Distributions of kinematic variables</b>	<b>28</b>
<b>C</b>	<b>Training uncertainty</b>	<b>30</b>
<b>D</b>	<b>Likelihood evaluation</b>	<b>31</b>

# 1 Introduction

More than ten years ago, the ATLAS and CMS collaborations announced the discovery of a new particle at a mass of about 125 GeV during Run-1 of the Large Hadron Collider (LHC) [1, 2]. Since its discovery in 2012, the quantum numbers of this Higgs boson have been tested extensively, as well as its interactions with other SM particles [3, 4]. Up to now, all results are in agreement with the predictions of the SM within the experimental and theoretical uncertainties. However, effects from beyond the Standard Model (BSM) physics could still be hidden in the current uncertainties and may be unveiled with the large amount of data to be collected during LHC Run-3 and the high-luminosity phase of the LHC (HL-LHC).

A so far relatively unconstrained property of the discovered Higgs boson is its behaviour under  $\mathcal{CP}$  transformations. This is of particular interest given that the amount of  $\mathcal{CP}$  violation present in the SM is — by several orders of magnitude — insufficient to explain the baryon asymmetry of the Universe [5, 6]. The possibility of the Higgs boson being a pure  $\mathcal{CP}$ -odd state was already ruled out shortly after its discovery by analyzing the  $\mathcal{CP}$  structure of its couplings to massive vector bosons [7, 8]. It is, nevertheless, still possible that the discovered Higgs boson is a mixed  $\mathcal{CP}$ -state instead of the  $\mathcal{CP}$ -even state predicted by the SM.

Electric dipole moments (EDMs) are sensitive probes of  $\mathcal{CP}$  violation beyond the SM [9, 10] and their experimental upper bounds, in particular of the electron [11, 12], neutron [13] and mercury [14], place strong constraints on  $\mathcal{CP}$ -violating Higgs interactions [15–19]. These constraints, however, strongly depend on the assumption about the first-generation Yukawa couplings [20], which themselves are only very weakly constrained [21, 22]. It is therefore of great interest to search for possible  $\mathcal{CP}$ -violating effects also at colliders, which allow for a distinction between different Higgs couplings.

At the LHC,  $\mathcal{CP}$ -violating Higgs interactions can be constrained either directly using  $\mathcal{CP}$ -odd observables or indirectly using  $\mathcal{CP}$ -sensitive, but  $\mathcal{CP}$ -even observables. While measuring a non-zero value for the former is an unambiguous sign of  $\mathcal{CP}$  violation, deviations in  $\mathcal{CP}$ -even observables are only indicative for  $\mathcal{CP}$  violation. On the other hand, it can be difficult to measure  $\mathcal{CP}$ -odd observables since it often requires measuring at least four independent momenta associated either with the Higgs production or with its decay (see e.g. Ref. [23]). In this situation, the measurement of  $\mathcal{CP}$ -sensitive observables can provide valuable complementary information.

The most stringent constraints on  $\mathcal{CP}$ -violating Higgs couplings so far have been set on the Higgs interactions with massive vector bosons [8, 24–32]. In most BSM theories,  $\mathcal{CP}$  violation in these interactions is expected to be loop-suppressed (given that a pseudoscalar cannot be coupled to massive vector bosons at the tree level).  $\mathcal{CP}$  violation in the Higgs interactions with fermions can, in contrast, occur unsuppressed. These are far less constrained with the existing experimental analyses targeting the Higgs interaction with tau leptons [33, 34] and with top quarks [30, 35–40].

Since the top-Yukawa coupling is of special interest due to its magnitude, also many

phenomenological studies have been carried out focusing mainly on top-associated Higgs production as a tree-level probe of the Higgs–top-quark interaction [18, 20, 41–74]. Besides that, the  $\mathcal{CP}$  character of the top-Yukawa coupling can also be probed by investigation of the Higgs production via gluon fusion (ggF). While ggF production alone (without the association of jets) is only sensitive to the  $\mathcal{CP}$  nature of the top-Yukawa interaction via its total rate, ggF production in association with one or two jets is more directly sensitive. In particular, Higgs production in association with two jets (ggF2j) is well known to be  $\mathcal{CP}$ -sensitive via the difference of the azimuthal angles of the two jets that enables the construction of a  $\mathcal{CP}$ -odd observable [47, 74–78].<sup>1</sup>

Generally, the ggF2j production does not directly probe the  $\mathcal{CP}$  structure of the top-Yukawa interaction but of the Higgs–gluon interaction. Conversely, a  $\mathcal{CP}$ -violating Higgs–gluon interaction cannot only be induced by a  $\mathcal{CP}$ -violating Higgs–top-quark interaction but also by  $\mathcal{CP}$ -violating Higgs interactions with coloured BSM states. Yet, given the increasingly strong limits on the mass scale of coloured BSM states set by experimental searches at the LHC [80–85], any sign for  $\mathcal{CP}$  violation in the Higgs–gluon interaction is plausible to originate at least partially from the Higgs–top-quark interaction. This makes the ggF2j channel not only interesting in its own respect, but also in the context of constraining the  $\mathcal{CP}$  structure of the effective Higgs–gluon interaction and the top-Yukawa coupling.

Existing experimental measurements so far only put relatively weak constraints on the  $\mathcal{CP}$  character of the Higgs–gluon interaction [29, 30, 37]. In this work, we investigate how these limits could be improved. In particular, we compare the potential of two distinct kinematic regions (a VBF-like and a ggF2j-like kinematic region) and use well-established machine-learning techniques (boosted classifiers) to identify whether a given event originates from a  $\mathcal{CP}$ -even interaction, a  $\mathcal{CP}$ -odd interaction, or from their interference. This allows us to construct both  $\mathcal{CP}$ -even and  $\mathcal{CP}$ -odd observables. In the ggF2j-like region, these show a significantly better sensitivity than the difference of the azimuthal angles of the two jets, which is widely used in the literature. Moreover, we highlight how the separation into two kinematic regions helps to distinguish  $\mathcal{CP}$  violation in the Higgs–gluon interaction from  $\mathcal{CP}$  violation appearing in the Higgs interaction with massive vector bosons.

The paper is structured as follows. In Section 2, we review Higgs production in association with two jets and introduce the effective theory that parameterizes our BSM couplings. Afterwards, we discuss the event generation and applied cuts in Section 3. Section 4 deals with the training setup of our classifiers. In this section, we also define the observables that are used to probe the  $\mathcal{CP}$ -structure of the Higgs–gluon coupling. We present expected exclusion limits in Section 5. The interplay of the  $\mathcal{CP}$  structure of the Higgs–gluon interaction with the  $\mathcal{CP}$  structure of the Higgs couplings with massive vector bosons is discussed in Section 6. The interpretation of our limits in terms of limit on the Higgs–top-quark interaction and a comparison to current experimental limits is shown in Section 7. Finally, Section 8 concludes our findings and gives a brief outlook into possible future studies.

---

<sup>1</sup>For ggF production in association with one jet, jet substructure information has to be exploited to construct a  $\mathcal{CP}$ -odd observable [79].

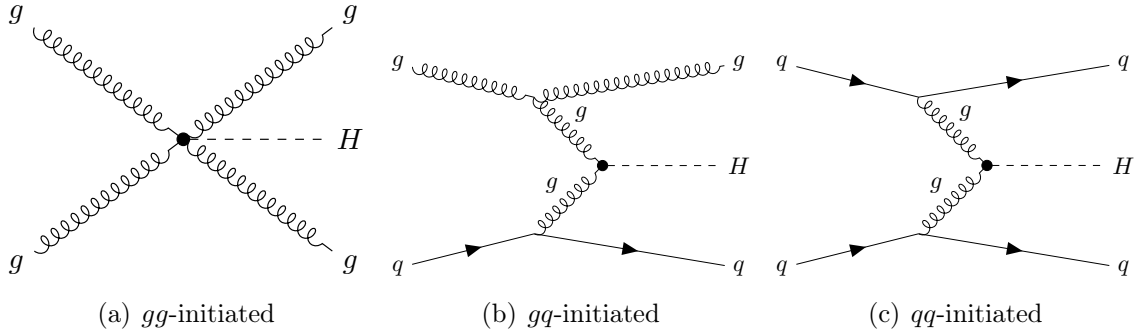


**Figure 1:** Example Feynman diagrams for the various ggF2j sub-channels.

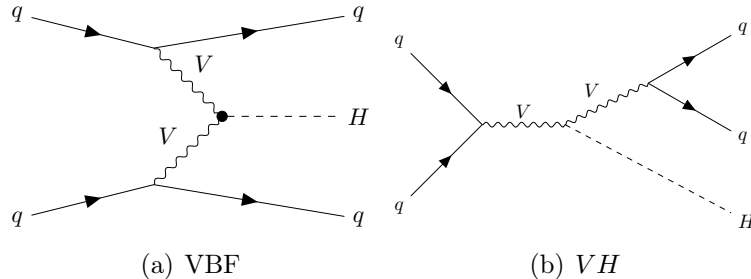


**Figure 2:** Exemplary Feynman diagrams for the considered background processes where  $V \in [W^+, W^-, Z]$  and  $q \in [q, \bar{q}]$ .

## 2 Gluon fusion with two jets in an EFT approach

Our work focuses on Higgs production with two jets. Here, we give an introduction to the relevant processes in the SM and then discuss our parameterization of BSM effects.

### 2.1 Gluon fusion in association with two jets

Higgs production via gluon fusion is the main production channel at the LHC with its cross section being (at minimum) an order of magnitude higher than any other Higgs production mode at  $\sqrt{s} = 13$  TeV. Even if two or more jets associated with the parton level interaction are required in the final state, the cross section is still higher than all other Higgs production modes [86] ( $\sigma_{\text{ggF}}^{j \geq 2} = 7.88$  pb and  $\sigma_{\text{VBF}} = 3.78$  pb at  $\sqrt{s} = 13$  TeV). In the SM, the gluon fusion process is induced mainly by a top-quark loop, while for our work we consider an effective point-like interaction with unknown  $\mathcal{CP}$  state (see Section 2.2).

The ggF2j process can be classified by its initial state, as can be seen in Fig. 1. The individual initial states with gluons have higher cross sections due to the larger contribution of the gluons compared to those of the quarks to the parton distribution functions (PDFs) of the proton. In our setup, we find that the  $gg$  initial state contributes  $\sim 72\%$  to the total ggF2j cross section, while the  $gq$  initial state still contributes  $\sim 26.5\%$ . The contribution of the  $qq$  initial state is very small ( $\sim 1.5\%$ ). We furthermore note that the interference

between the  $qq$ -induced ggF2j production and Higgs production via VBF was found to be negligible [87, 88].

Example Feynman diagrams for the considered background (BG) processes — VBF and  $VH$  production — are shown in Fig. 2.

## 2.2 Effective Higgs-vector boson interactions

We perform our study in an effective field theory (EFT) framework. Following Ref. [89], we parameterize the interaction of the Higgs boson with gluons in the following form,

$$\mathcal{L}_{ggH} = -\frac{1}{4v} \left( -\frac{\alpha_s}{3\pi} c_g G_{\mu\nu}^a G^{\mu\nu,a} + \frac{\alpha_s}{2\pi} \tilde{c}_g G_{\mu\nu}^a \tilde{G}^{\mu\nu,a} \right) H, \quad (1)$$

where  $H$  is a Higgs field,  $G_{\mu\nu}^a$  is the gluon field strength tensor,  $v = 246$  GeV is the vacuum expectation value and  $\alpha_s = g_s^2/4\pi$  is the strong coupling constant. Here, we assume that this interaction already includes the Higgs–gluon vertex induced by the top quark in the infinite top-mass limit.<sup>2</sup> Accordingly,  $c_g = 1$  and  $\tilde{c}_g = 0$  in the SM. Deviations from the SM can either be induced by a modified top-Yukawa coupling or by coloured BSM particles.

The prefactors of the operators are chosen such that modifications of the top-Yukawa interaction directly map to the operators of Eq. (1) if we assume that no coloured BSM particles affect the Higgs–gluon interaction. In this case, we have  $c_g = c_t$  and  $\tilde{c}_g = \tilde{c}_t$  in the infinite top-quark mass limit, if we parameterize the top-Yukawa interaction via

$$\mathcal{L}_{\text{top-Yuk}} = -\frac{y_t^{\text{SM}}}{\sqrt{2}} \bar{t}(c_t + i\gamma_5 \tilde{c}_t)tH, \quad (2)$$

where  $y_t^{\text{SM}}$  is the SM top-Yukawa interaction and  $c_t = 1$  as well as  $\tilde{c}_t = 0$  for the SM.

We account for effects due to the finite mass of the top quark by rescaling the total rate and placing an upper bound on the Higgs transverse momentum (see Section 3).

The modified Higgs-gluon coupling of Eq. (1) affects ggF2j production. Its matrix element can be separated into three pieces

$$\left| \mathcal{M}_{\text{ggF2j}} \right|^2 = c_g^2 \left| \mathcal{M}_{\text{even}} \right|^2 + 2c_g \tilde{c}_g \text{Re} \left[ \mathcal{M}_{\text{even}} \mathcal{M}_{\text{odd}}^* \right] + \tilde{c}_g^2 \left| \mathcal{M}_{\text{odd}} \right|^2. \quad (3)$$

The first and third terms proportional to the squared values of the coupling modifiers are  $\mathcal{CP}$ -even, while the second term parameterizing the interference between the two  $\mathcal{CP}$ -states is  $\mathcal{CP}$ -odd.  $\mathcal{CP}$  violation in the Higgs-gluon interaction is therefore only realised for a non-zero value of the interference term. Correspondingly, the interference term gives a non-zero contribution only for distributions of  $\mathcal{CP}$ -odd observables.

---

<sup>2</sup>In other works (see e.g. Refs. [30, 37], the Higgs–gluon interaction is written in the form  $\mathcal{L}_{ggH} = -\frac{\alpha_s \pi}{v} \left( c_{gg} G_{\mu\nu}^a G^{\mu\nu,a} + \tilde{c}_{gg} G_{\mu\nu}^a \tilde{G}^{\mu\nu,a} \right) H$  without including the effect of the top-quark loop. In the infinite top-quark mass limit, both parameterizations are related via  $c_g = 1 + 12\pi^2 c_{gg}$  and  $\tilde{c}_g = -8\pi^2 \tilde{c}_{gg}$ .

In addition to a modification of the Higgs–gluon interaction, in Section 6 we will also consider a  $\mathcal{CP}$ -violating interaction of the Higgs boson with massive vector bosons. We parameterize this interaction as<sup>3</sup>

$$\mathcal{L}_{\Phi VV} = \mathcal{L}_{\text{gauge}} + \frac{c_{\Phi\widetilde{W}}}{\Lambda^2} \mathcal{O}_{\Phi\widetilde{W}} \quad \text{with} \quad \mathcal{O}_{\Phi\widetilde{W}} \equiv \Phi^\dagger \Phi \widetilde{W}_{\mu\nu} W^{\mu\nu}, \quad (4)$$

where  $\mathcal{L}_{\text{gauge}}$  is the SM gauge Lagrangian.  $W$  and  $\widetilde{W}$  are the  $SU(2)_L$  field strength and its dual, respectively.  $\Phi$  is the Higgs doublet and  $\Lambda$  denotes the cut-off scale of the EFT, which we set to 1 TeV. If not stated otherwise, we will for the main part of this work assume that  $c_{\Phi\widetilde{W}} = 0$  such that the Higgs coupling to massive vector bosons is SM-like.

### 3 Event generation

As discussed in Section 1, we focus on Higgs production via gluon fusion in association with two jets, which we refer to as ggF2j in the following. This production channel offers a unique sensitivity to probe the  $\mathcal{CP}$  nature of the Higgs–gluon interaction. Moreover, in this work, we concentrate on the Higgs decay to two photons. While this simplifies our analysis, our general analysis strategy can be straightforwardly adapted to other Higgs decay channels.

The main background processes are Higgs production via vector-boson fusion (VBF) and Higgsstrahlung ( $VH$ ). Additionally, there is a continuous background from the  $qq \rightarrow qq$  process with two photons from final state radiation. However, this background can be subtracted by a fit to the smoothly falling di-photon mass distribution. In recent measurements of the  $H \rightarrow \gamma\gamma$  decay channel, the modelling of this background was responsible for only an uncertainty of 1.3% to the total signal rate, which is minor compared to other experimental uncertainties [91]. Therefore, we expect the impact of this subtraction on our analysis to be small and neglect the continuous background in our work.

Events are generated at parton level with MadGraph5\_aMC@NLO (version 3.4.0) [92] and are passed on to Pythia8 (version 8.306) [93] and Delphes3 (version 3.4.2) [94] for parton showering, hadronisation and detector simulation. For the detector simulation with Delphes3, we employ the ATLAS detector card with a modified jet cone radius of  $\Delta R = 0.4$  which is more widely used in experimental analyses. A jet is then defined as a set of particles in this cone which in total reach a minimum of  $p_T^j \geq 20$  GeV, with the particles having passed an electron, muon, photon and neutrino filter before. Reconstruction of the jet is performed using the anti- $k_t$  algorithm [95]. Photons (which are used for reconstructing the Higgs boson) are identified by observing electrons and muons in a cone with radius  $\Delta R = 0.5$  and momentum  $p_T \geq 0.5$  GeV. More details on the event generation and the employed UFO model [96, 97] can be found in Appendix A.

We generate data sets for Higgs production from the ggF2j, VBF and  $VH$  processes. While the latter two do not receive any BSM contribution in our model, the event generation

---

<sup>3</sup>At dimension six in the SM effective field theory (SMEFT), three distinct operators can introduce  $\mathcal{CP}$  violation in VBF production (see e.g. Ref. [90]). In this work, we concentrate on the  $\mathcal{O}_{\Phi\widetilde{W}}$ . We expect similar results for the other operators.

Applied cut	Fraction of accepted events				
	ggF2j $ \mathcal{M}_{\text{even}} ^2$	ggF2j Interf.	ggF2j $ \mathcal{M}_{\text{odd}} ^2$	VBF	$VH$
Initial events	100%	100%	100%	100%	100%
$N_j \geq 2; N_\gamma \geq 2$	48.1%	50.8 %	48.1%	62.6%	49.8%
$110 \text{ GeV} \leq m_{\gamma\gamma}$ $m_{\gamma\gamma} \leq 140 \text{ GeV}$	47.8%	50.5%	47.9%	62.0%	49.4%
$p_T^{\gamma^1}/m_{\gamma\gamma} \geq 0.35$ $p_T^{\gamma^2}/m_{\gamma\gamma} \geq 0.25$	39.4%	40.9%	39.8%	50.0%	40.5%
$p_T^{j^1} \geq 30 \text{ GeV}$ $p_T^{j^2} \geq 20 \text{ GeV}$	38.6%	40.2%	38.6%	49.7%	39.9%
$ \eta_j  \leq 2.5$ $ \eta_\gamma  \leq 2.5$	22.9%	21.5%	22.7%	39.8%	31.2%
$p_T^H \leq 200 \text{ GeV}$	18.6%	18.4%	18.3%	34.4%	26.8%

**Table 1:** Cutflow table for the Higgs production mechanisms considered in this work. Listed are all cuts applied after the event generation, along with the percentage of events that survives the cut.



of ggF2j production is split into three terms following the parameterization in Eq. (3). We therefore obtain separate data sets for the terms proportional to  $c_g^2$  (the  $\mathcal{CP}$ -even amplitude squared),  $\tilde{c}_g^2$  (the  $\mathcal{CP}$ -odd amplitude squared), and  $c_g\tilde{c}_g$  (the interference between the  $\mathcal{CP}$ -even and  $\mathcal{CP}$ -odd amplitude). This amounts to five distinct classes which we further split into independent data sets for training, validating and testing the classifiers, which will be introduced in Section 4.

Before training the classifiers, we impose a number of simple baseline cuts mimicking the event selection typically used by ATLAS and CMS for  $H \rightarrow \gamma\gamma$  measurements [35, 36]. A cutflow table detailing the imposed cuts and the corresponding reduction in the event numbers can be found in Table 1, where the percentage of acceptance after each cut is displayed for all signal and background processes examined in this work.

First of all, a cut on  $N_j$  and  $N_\gamma$  ensures that at least two jets and two photons are found in each event, which are needed to reconstruct the Higgs boson and identify ggF2j production. Only accepting events with  $110 \text{ GeV} \leq m_{\gamma\gamma} \leq 140 \text{ GeV}$  ensures that a Higgs boson is present in the event and suppresses any non-Higgs background. The cuts on low values of  $p_T^\gamma$  and  $p_T^j$  suppress misidentified photons and jets that do not originate from the parton level interaction. Finally, only events with  $|\eta_j| \leq 2.5$  and  $|\eta_\gamma| \leq 2.5$  are accepted to match the pseudorapidity coverage of the ATLAS inner detector. As an additional requirement, we place an upper limit of  $p_T^H \leq 200 \text{ GeV}$  on the Higgs transverse momentum (reconstructed out of the two photon momenta). This cut ensures that the top-quark loop inducing ggF2j production cannot be resolved and ggF2j production can be reliably interpreted using the effective Lagrangian given in Eq. (1) (see e.g. discussion in Ref. [98]).

As the cutflow in Table 1 shows, the cut on  $p_T^H$  reduces the number of surviving events by 14 – 19%. While this reduction is not a critical limitation for our analysis, in principle one can include the events with higher  $p_T^H$  beyond the infinite top-quark mass limit by employing the  $\text{FT}_{\text{approx}}$  approximation [99]. This approximation combines the exact top-quark mass and width in the Born, one-loop and real amplitudes with approximated and re-scaled two-loop virtual contributions, originally applied to multi-Higgs production. The  $\text{FT}_{\text{approx}}$  approximation has been successfully validated against the full NLO calculation in the SM for  $H + j$  production [100]. Under the assumption that the  $\text{FT}_{\text{approx}}$  approximation yields similarly accurate results for Higgs production in association with a higher multiplicity of jets, Ref. [100] has also improved the calculation of differential cross sections for  $H + 2j$  by complementing the exact real corrections with the approximated two-loop virtual corrections. The good agreement between their NLO result in the heavy-top limit (HTL) and in the  $\text{FT}_{\text{approx}}$  up to  $p_T^H \leq 300 \text{ GeV}$  justifies our treatment in the HTL within the chosen cut on  $p_T^H$ . The relevance of the finite top-quark mass at higher  $p_T^H$  and the success of  $\text{FT}_{\text{approx}}$  in  $H + j$  motivate a future study of  $\mathcal{CP}$  properties of the Higgs boson without cutting out the high- $p_T^H$  events. For the scope of our work, our robust treatment with the  $p_T^H$ -cut results in conservative limits that might be improved by a refined event generation.

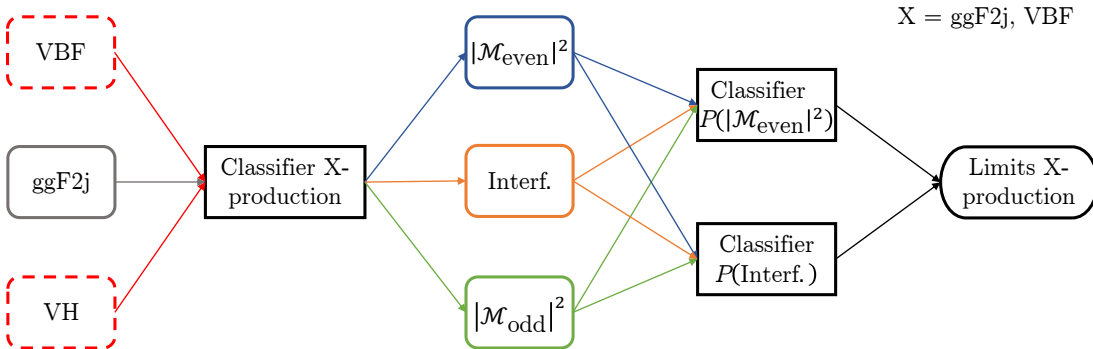


**Figure 3:** Outline of the strategy for this analysis. First, a classifier is trained for signal and background separation for each of the two considered Higgs production processes  $X = \{\text{ggF2j}, \text{VBF}\}$ . Afterwards, the obtained data in the respective kinematic region are used in two classifiers each, where one of them learns a  $\mathcal{CP}$ -even and the other one a  $\mathcal{CP}$ -odd observable.

## 4 Analysis strategy

Our analysis is structured into two steps. In the first step, two distinct classifiers are trained to separate the events originating from the different Higgs production channels. One classifier is trained to separate the signal events (from ggF2j production) from the relevant background processes, while the other is trained to recognize VBF events. The scores of these classifiers are used to define two signal regions (SR), one containing ggF2j-like events and the other containing VBF-like events. Both SRs offer possible advantages in the analysis. In the ggF2j-SR, we expect an increased sensitivity as it contains significantly more events than the VBF-SR. However, the ggF2j events with a  $q\bar{q}$  initial state share the topology of VBF Higgs production and were shown to carry the most  $\mathcal{CP}$  information after applying typical VBF-cuts in an earlier work Ref. [76].

Both classifiers are trained on the same input data. Since the two classifiers are independent, it is possible for events to appear in both or none of the kinematic regions. For our data set, the percentage of ggF2j data that appear in both the ggF2j-SR and the VBF-SR is about 8% of the total data set, while about 11% of the events do not appear in either of them. Subsequently, the events identified in each category are passed to two additional classifiers (see description below). These are used to distinguish the squared  $\mathcal{CP}$ -odd and  $\mathcal{CP}$ -even matrix elements and the interference term in the ggF2j production (see Eq. (3)) and thereby to construct  $\mathcal{CP}$ -sensitive observables. The analysis steps for each of the kinematic regions are summarized in Fig. 3.

## 4.1 Signal-background separation

As mentioned above, two classifiers are trained to define a ggF2j- and a VBF-SR with distinct kinematics. In both cases, we reduce the separation to a binary classification problem, where the respective signal is trained against all other types of events. The classifiers are set up with PyTorch and the same data set is used for training, validation, and testing of both classifiers.

The following kinematic variables are used as input for the signal-background separation:

- the energy  $E$ , the transverse momentum  $p_T$ , the pseudorapidity  $\eta$ , and the azimuthal angle  $\phi$  of the Higgs boson and the two leading- $p_T$  jets,
- the invariant mass of the two leading- $p_T$  jets  $m_{jj}$ , their pseudorapidity difference  $\Delta\eta_{jj}$ , and their azimuthal angle difference  $\Delta\phi_{jj}$  (where the sign is chosen such that the  $\phi$  of the jet with the smaller  $\eta$  is subtracted from the one with larger  $\eta$ ),
- the number of jets in the event  $N_j$ , and
- the respective energy  $E$  of each jet that is not leading or sub-leading in  $p_T$ .

Among the most important variables for the signal/background separation are  $N_j$ ,  $m_{jj}$ ,  $|\Delta\eta_{jj}|$ , and  $\Delta\phi_{jj}$  (see e.g. Ref. [47]). It can be seen that the three processes (ggF2j, VBF and  $VH$ ) show quite distinct topologies which are important for training the NN. While the usage of higher-level observables (like  $|\Delta\eta_{jj}|$  and  $m_{jj}$ ) does not provide the classifiers with new information, they can still be useful in order to improve the training process. Such observables should, however, only be included if they are expected or known to impact the outcome of the classifier, as they can slow down the training otherwise. In the present case,  $|\Delta\eta_{jj}|$  and  $m_{jj}$  are well-known examples for variables allowing one to distinguish the events stemming from VBF and ggF2j production.

The classifier creating the ggF2j-SR (VBF-SR) reaches an accuracy of about 70% (79%). The classifier score, which gives an estimate of the probability for each event to be a signal event, is calculated for ggF2j, VBF and  $VH$  Higgs production, respectively, and plotted in Fig. 4(a) (Fig. 4(b)). The ggF2j production is additionally split up into the three possible initial states ( $qq$ ,  $gq$  and  $gg$ ). We observe that the more quarks are in the initial state, the more likely it is for an event to be classified as VBF. Especially for the  $qq$  initial state, this can be easily understood by comparing the example Feynman diagrams in Fig. 1(c) and Fig. 2(a), which only differ via the exchange of the gluon/heavy vector boson propagators creating the Higgs. We additionally observe that interference events from ggF2j are more likely to be identified as VBF-like events than events from the squared terms are.

For both classifiers, the respective signal process is the dominant process for a score of  $P(\text{signal}) \gtrsim 0.5$  and we therefore set  $P(\text{signal}) \geq 0.5$  as a cut to define our SRs. All accepted events are combined into a new data set and subsequently passed on to two additional classifiers, in order to gain information about their  $\mathcal{CP}$  structure.

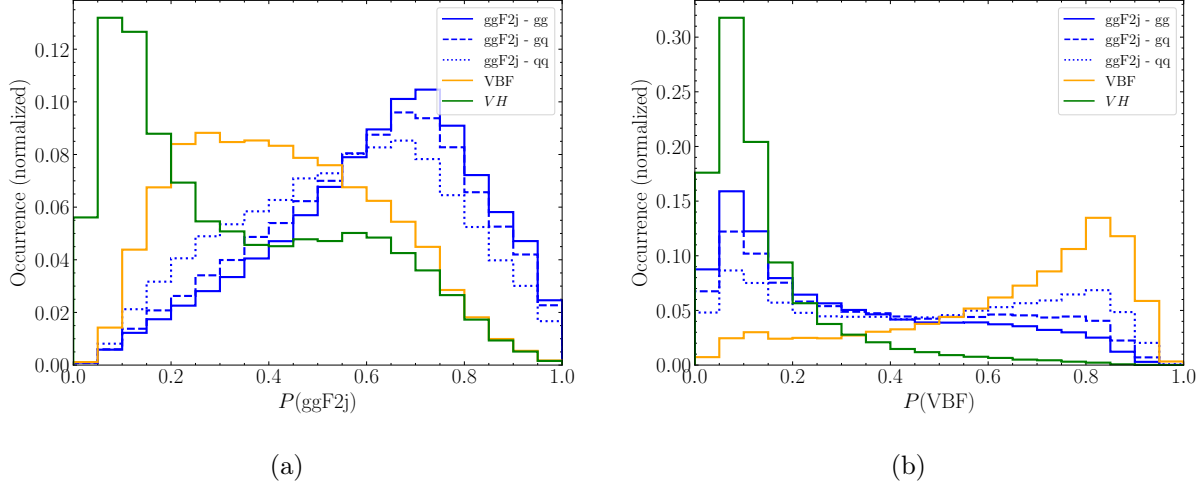


**Figure 4:** Scores of the trained classifiers for defining a (a) ggF2j and (b) VBF signal region for the different production channels.

## 4.2 Separating the different ggF2j contributions

The three terms in the squared ggF2j amplitude in Eq. (3) can be probed by exploiting rate information as well as their different kinematics. The interference term can only be probed by  $\mathcal{CP}$ -odd observables since its positive and negative contributions cancel out for  $\mathcal{CP}$ -even observables. One such observable is  $\Delta\phi_{jj}$ , which has been used as a  $\mathcal{CP}$  observable in previous analyses (see e.g. Ref. [29]). Fig. 5 shows the contributions of the squared and interference terms to the differential cross section, plotted against  $\Delta\phi_{jj}$ . Since  $\Delta\phi_{jj}$  is a  $\mathcal{CP}$ -odd observable, the distribution for the interference term is antisymmetric, while the distribution of the squared  $\mathcal{CP}$ -even and  $\mathcal{CP}$ -odd matrix elements are symmetric. We impose a  $\mathcal{CP}$  flip on the events<sup>4</sup> before the training to ensure the symmetry of the distributions even for a limited number of Monte-Carlo events. The two peaks close to  $\Delta\phi_{jj} = 0$  in the ggF2j-SR originate from events with low  $m_{jj}$  and vanish if a minimal  $m_{jj}$  cut is imposed.

For the training of the  $\mathcal{CP}$  classifiers, we use the full kinematic information of the two leading jets and the reconstructed Higgs boson, as well as  $m_{jj}$ ,  $\Delta\eta_{jj}$ , and  $\Delta\phi_{jj}$  as additional high-level observables. The distributions of all variables used in the training can be found in Appendix B where they are split up into the three possible contributions to the ggF2j cross section. Compared to the signal-background separation, we dropped the information about additional jets, since these were found to carry little to no information about the  $\mathcal{CP}$  character of the Higgs–gluon interaction. For the  $\mathcal{CP}$  classification, we used the **Gradient Boosting Classifier** from the `scikit-learn` [101] package. We train two classifiers independently for each of the signal regions defined by the signal-background classifiers. Two observables are constructed from their output in the following way:

<sup>4</sup>This corresponds to flipping the sign of the particle momenta as well as in case of the interference term the weight on an event-by-event basis.

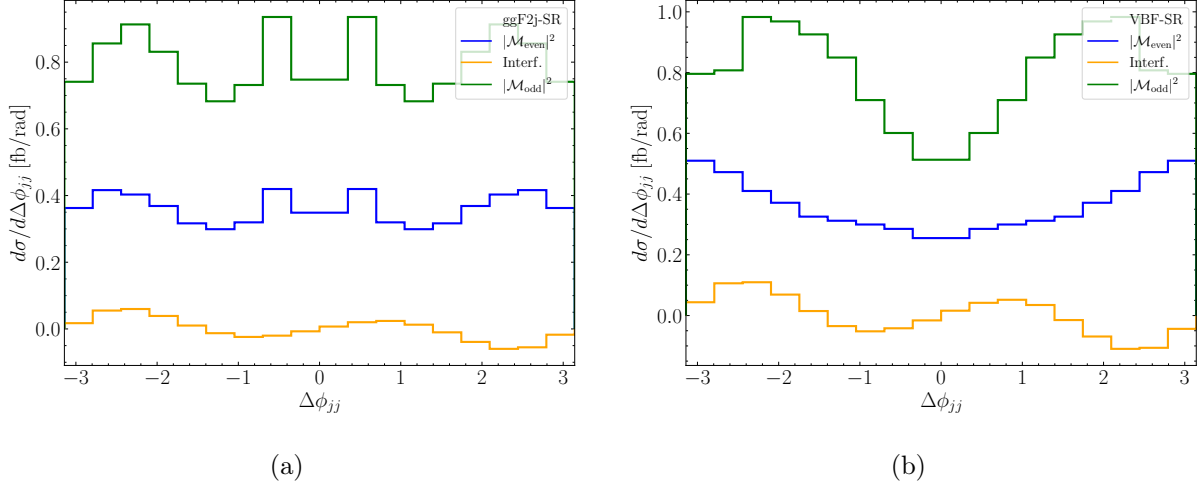
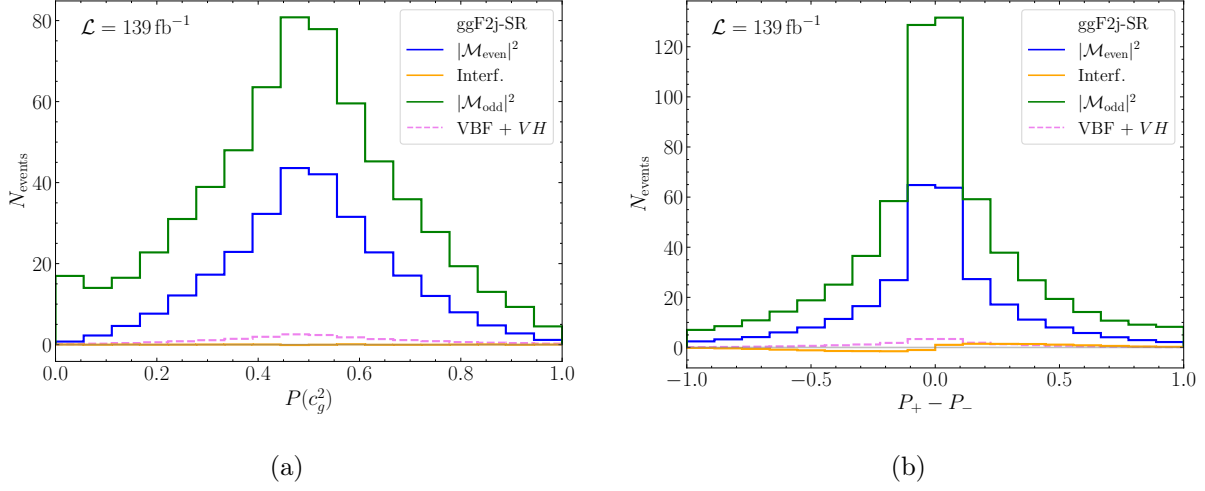


**Figure 5:** The differential cross section as a function of  $\Delta\phi_{jj}$  in the (a) ggF2j- and (b) VBF-SR, plotted for the  $|\mathcal{M}_{\text{even}}|^2$  (blue), interference (orange) and  $|\mathcal{M}_{\text{odd}}|^2$  (green) contributions.

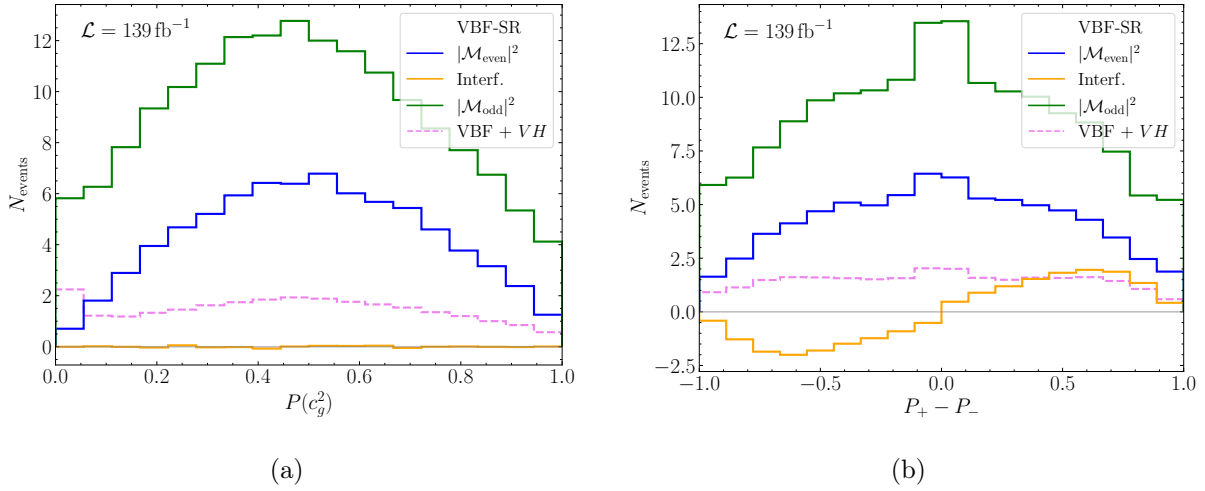
- The first classifier only separates between the squared  $\mathcal{CP}$ -even and the squared  $\mathcal{CP}$ -odd terms. The corresponding output observable is defined as  $P(c_g^2)$ , which can be interpreted as a probability that a given event originates from the  $|\mathcal{M}_{\text{even}}|^2$  contribution.
- The second classifier deals with the interference term. It is trained to separate positive and negative interference events as well as to distinguish these from events originating from either of the squared terms. Following Ref. [102], the observable built from the output is defined as  $P_+ - P_-$  where  $P_+$  ( $P_-$ ) is the probability of an event to correspond to positive (negative) interference. This observable is  $\mathcal{CP}$ -odd by definition.

Fig. 6 shows the output of the two  $\mathcal{CP}$  classifiers in the ggF2j-SR. Each classifier has been trained 100 times (see Appendix C) and here we show the one with the strongest constraints on the Higgs-gluon coupling modifiers (see Section 5.1). For the  $P(c_g^2)$  classifier, this corresponds to the case in which the difference between the squared terms was learned best. The classifier learning the interference terms showed only very slight fluctuations during the training processes. Since its output is a  $\mathcal{CP}$ -odd observable by construction, the squared ggF2j contributions, as well as BG contributions, show the expected behaviour of being symmetric around zero. The interference contribution is asymmetric around zero. Its amplitude compared to the squared contributions is very small due to its small cross section, an overall lower number of interference events in the ggF2j-SR from the signal-background separation, and misidentified events during the  $\mathcal{CP}$  classification.

The output of the  $\mathcal{CP}$  classifiers in the VBF-SR is plotted in Fig. 7. Again, we show the distributions of the classifiers yielding the strongest limits (see Section 5.2) after 100 training iterations. Here, the visible statistical fluctuations in the  $|\mathcal{M}_{\text{even}}|^2$  and  $|\mathcal{M}_{\text{odd}}|^2$  contributions



**Figure 6:** Distributions of the two  $\mathcal{CP}$  discriminants (see text for the definition) for the classifiers yielding the strongest limits on the coupling modifiers in the ggF2j-SR.



**Figure 7:** Distributions of the two  $\mathcal{CP}$  discriminants for the classifiers giving the strongest limits on the coupling modifiers in the VBF-SR.

arise due to the comparably low number of ggF2j events in this signal region. In contrast, the asymmetry of the interference term in the  $P_+ - P_-$  observable is much more visible. Even in the VBF-SR, the number of BG events (consisting of VBF and VH events) is still lower than the number of ggF2j events, which is a consequence of the smaller cross section.

## 5 Sensitivity to the Higgs–gluon coupling

In this section, we present expected limits on the Higgs–gluon coupling, individually for the two signal regions as well as in a combined form. Details on the parameter fit can be found in Appendix D. Furthermore, we evaluate the impact of individual observables on the expected limits.

### 5.1 ggF2j signal region

We first present our results in the ggF2j-SR, where the contributions from background processes are strongly suppressed by the signal-background classifier. Expected limits are derived under the assumption that the data is SM-like for a luminosity of  $139 \text{ fb}^{-1}$ . This fit is based on the binned distribution of the various observables. The results are then plotted in the  $(c_g, \tilde{c}_g)$  parameter plane.

First, we show the limits obtained from the  $\Delta\phi_{jj}$  distribution (see Fig. 5(a)) in Fig. 8(a). It can be seen that the allowed parameter space is constrained to the form of an ellipse for which the ggF2j total rate is close to its SM value. The  $\Delta\phi_{jj}$  observable alone is not able to exclude any region of this ellipse within the  $1\sigma$  region.

The limits from the two classifiers are obtained from Fig. 6(a) and Fig. 6(b), respectively. The  $P(c_g^2)$  observable provides by far the strongest constraints among the two observables constructed from the classifiers (see Fig. 8(b)). Here, the ellipse is split up within the  $3\sigma$  region, which constrains the  $\mathcal{CP}$ -odd Higgs–gluon coupling  $\tilde{c}_g$  to the interval  $[-0.35, 0.35]$  at the  $1\sigma$  level. While the  $P_+ - P_-$  observable based on the interference contribution leads to weaker constraints (see Fig. 8(c)), it still outperforms the  $\Delta\phi_{jj}$  variable. Computing the limits from a two-dimensional histogram with both  $\mathcal{CP}$ -observables shows a small improvement over the  $P(c_g^2)$  limit (see Fig. 8(d)), limiting  $\tilde{c}_g \in [-0.32, 0.32]$  at the  $1\sigma$  level.

### 5.2 VBF signal region

Since the VBF-SR contains significantly more VBF events than the ggF2j-SR, the difference in the rate between the BSM and SM scenarios, which both contain the same VBF and VH events, is reduced compared to the ggF2j-SR. This is reflected in Fig. 9 where the ellipse is now wider.

Just like in the ggF2j-SR, the  $\Delta\phi_{jj}$  variable in Fig. 9(a) is not able to exclude part of the ellipse. In contrast to the previous results, the  $P(c_g^2)$  observable gives very similar limits to  $\Delta\phi_{jj}$  (see Fig. 9(b)). The interference classifier (see Fig. 9(c)) again results in

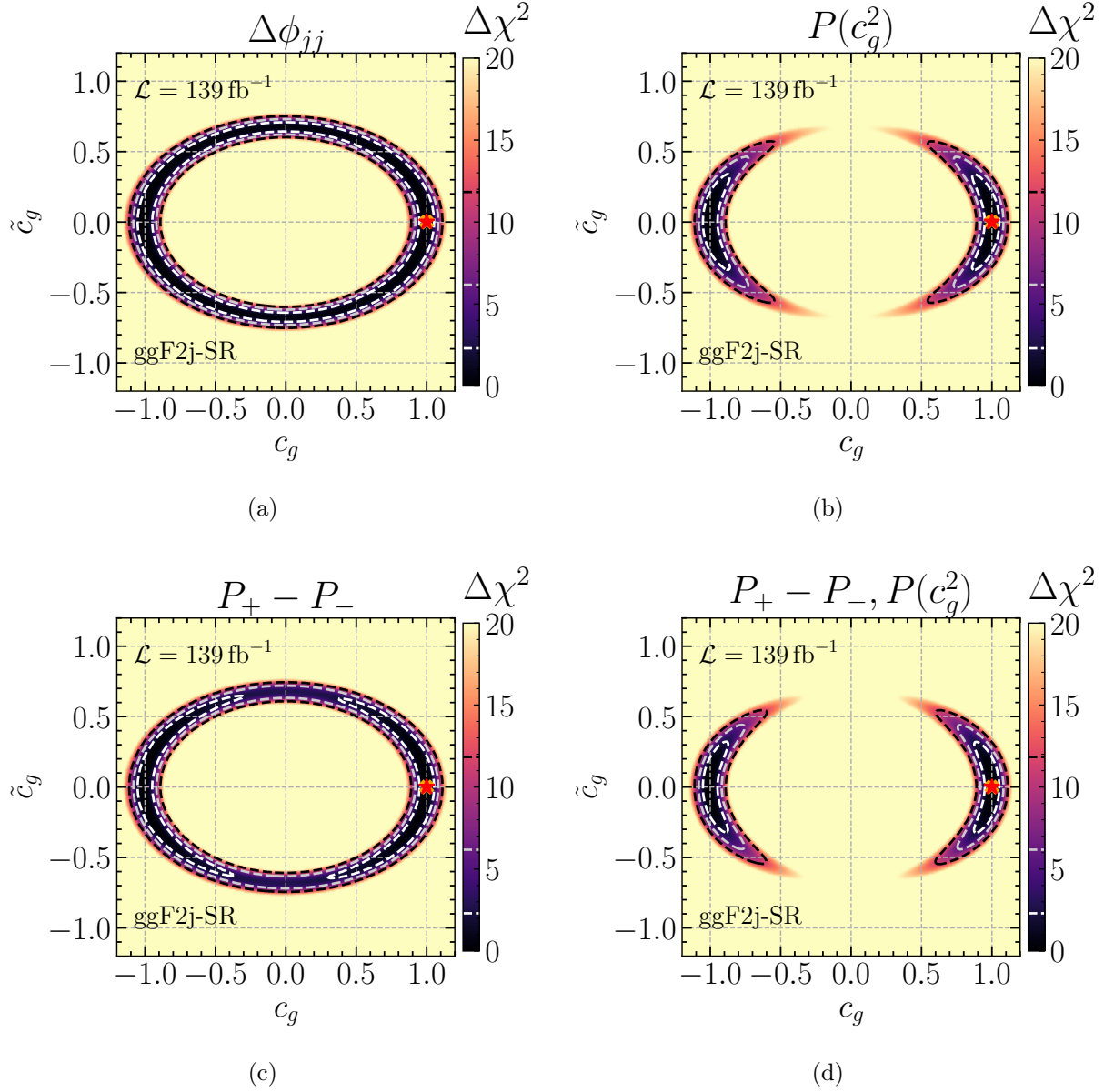


**Figure 8:** Limits from (a)  $\Delta\phi_{jj}$ , (b) the classifier trained to distinguish  $|\mathcal{M}_{\text{even}}|^2$  vs.  $|\mathcal{M}_{\text{odd}}|^2$ , (c) the classifier trained to distinguish positive vs. negative interference, and (d) the combined limits from both classifiers. All limits are shown for the ggF2j-SR. The 1-, 2- and 3- $\sigma$  contours are marked by white, grey and black dashed lines, respectively. The SM is marked by an orange cross and the best-fit (BF) point by a red star.



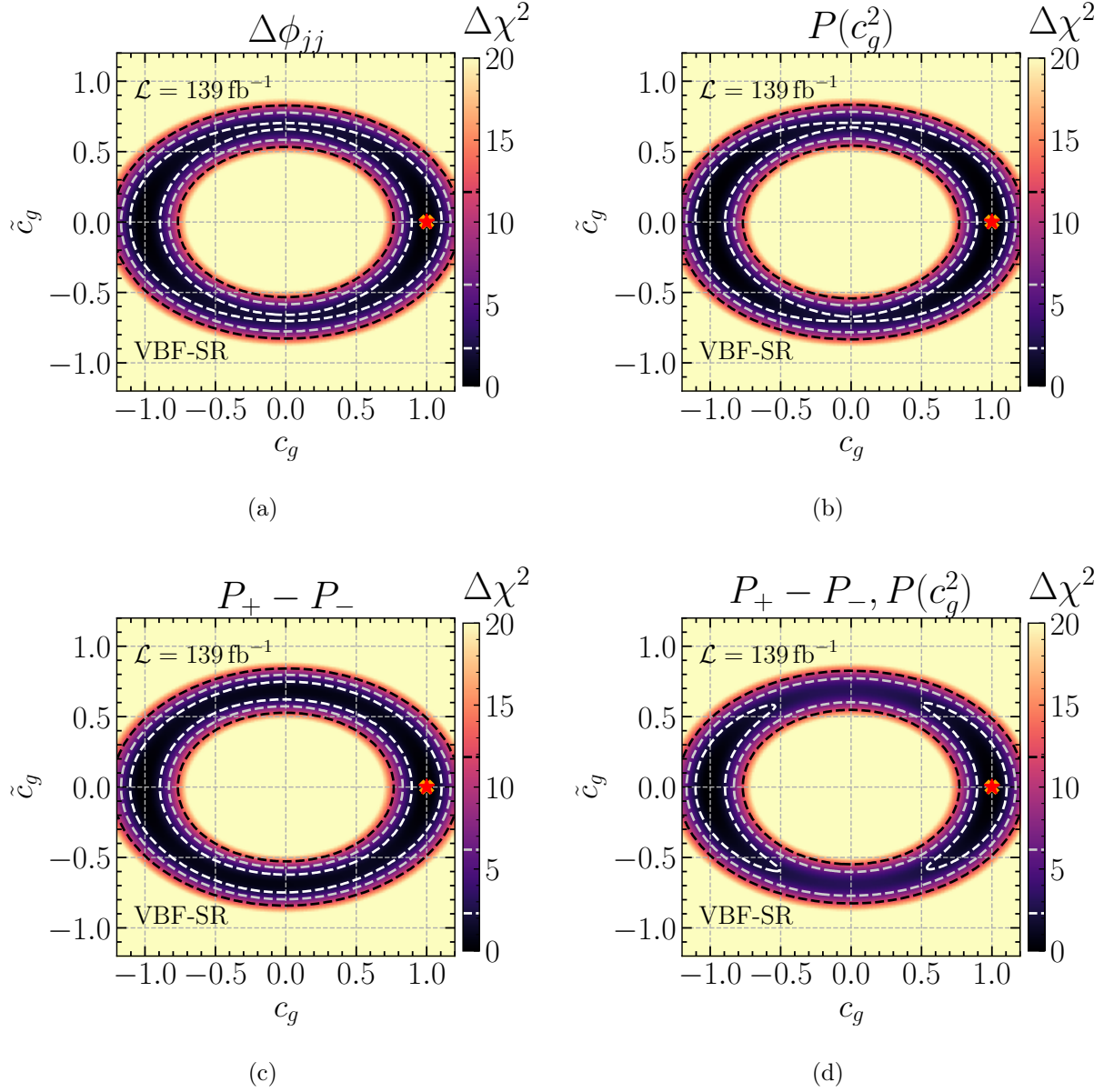


**Figure 9:** Limits from (a)  $\Delta\phi_{jj}$ , (b) the classifier trained to distinguish  $|\mathcal{M}_{\text{even}}|^2$  vs.  $|\mathcal{M}_{\text{odd}}|^2$ , (c) the classifier trained to distinguish positive vs. negative interference and (d) the combined limits from both classifiers. All limits are shown for the VBF-SR. The 1-, 2- and 3- $\sigma$  contours are marked by white, grey and black dashed lines, respectively. The SM is marked by an orange cross and the BF point by a red star.

worse limits than the  $P(c_g^2)$  observable, but now even worse limits than  $\Delta\phi_{jj}$ . This can be understood by taking into account which information each of the observables is provided with. While the classifiers directly use  $\Delta\phi_{jj}$  during the training process, the classifier training  $|\mathcal{M}_{\text{even}}|^2$  vs.  $|\mathcal{M}_{\text{odd}}|^2$  is missing the information about the interference contribution. This effect is negligible in the ggF2j-SR due to the small amplitude of the interference term, but it is non-negligible here (see Fig. 6(b) and Fig. 7(b)). On the other hand, the interference classifier does not differentiate between the  $|\mathcal{M}_{\text{even}}|^2$  and  $|\mathcal{M}_{\text{odd}}|^2$  contributions. Finally, the combination of both classifiers (see Fig. 9(d)), which uses the full information about the contributing terms to  $\sigma_{\text{ggF2j}}$ , puts stronger constraints on the Higgs–gluon coupling modifiers than  $\Delta\phi_{jj}$ . In contrast to the ggF2j-SR, the improvement over  $\Delta\phi_{jj}$  is, however, not so significant. This highlights the high sensitivity of the  $\Delta\phi_{jj}$  variable in the VBF-SR (see also the discussion in Section 5.4). We obtain  $\tilde{c}_g \in [-0.58, 0.58]$  for the best classifier in this signal region.

### 5.3 Combination

We now evaluate how the constraints on the Higgs–gluon coupling modifiers change when we combine the ggF2j-SR and the VBF-SR. The limits obtained from the  $P(c_g^2)$  and  $P_+ - P_-$  classifiers can be found in Fig. 10(a) and Fig. 10(b), respectively. The limits combining the  $P(c_g^2)$  and  $P_+ - P_-$  classifiers are depicted in Fig. 10(c). The  $1\sigma$  ( $2\sigma$ ) limit is shown as a dashed (dotted) line for the ggF2j-, the VBF- and the combined SRs. As the plots display, the combination of both SRs leads to an advantage over the single ggF2j-SR only for the interference classifier. In contrast to this, the limits from the  $P(c_g^2)$  observable in the combined region are slightly weaker than in the ggF2j-SR alone. These opposite effects of the combined SR on the two classifiers originate from a different fraction of the ggF2j, VBF and  $VH$  events when adding the events from the VBF-SR to the ggF2j-SR: The relative number of both VBF events and ggF2j interference events is increased, as the latter make up the majority of misidentified ggF2j events in the VBF-SR. The limits obtained from using both classifier observables are not affected when combining both signal regions, see Fig. 10(c).

The expected limits at different benchmark luminosities corresponding to Run-2 and Run-3 of the LHC and further the HL-LHC are depicted in Fig. 10(d). We note that the improvement of the limits with increased luminosity is slightly worse than naively expected ( $\propto 1/\sqrt{\mathcal{L}}$ ). This is a consequence of the suppression of the  $|\mathcal{M}_{\text{odd}}|^2$  contribution close to the SM point as well as the small impact of the interference term. We expect the limits at the  $2\sigma$  level to improve from  $\tilde{c}_g \in [-0.44, 0.44]$  at  $\mathcal{L} = 139 \text{ fb}^{-1}$  to  $\tilde{c}_g \in [-0.35, 0.35]$  at  $\mathcal{L} = 300 \text{ fb}^{-1}$  and  $\tilde{c}_g \in [-0.2, 0.2]$  at  $\mathcal{L} = 3000 \text{ fb}^{-1}$ , respectively.

In comparison to the expected limits from existing experimental analyses [29, 30, 37], our combined limit is significantly stronger. In particular, Refs. [29, 30, 37] are not sensitive to the  $\mathcal{CP}$  structure of the Higgs–gluon interaction at the  $2\sigma$  level. While these analyses focus on other Higgs decay channels, there are additional important differences: In Refs. [30, 37], the analysis is restricted to a VBF-like signal region. In Ref. [29], the limit is based solely on

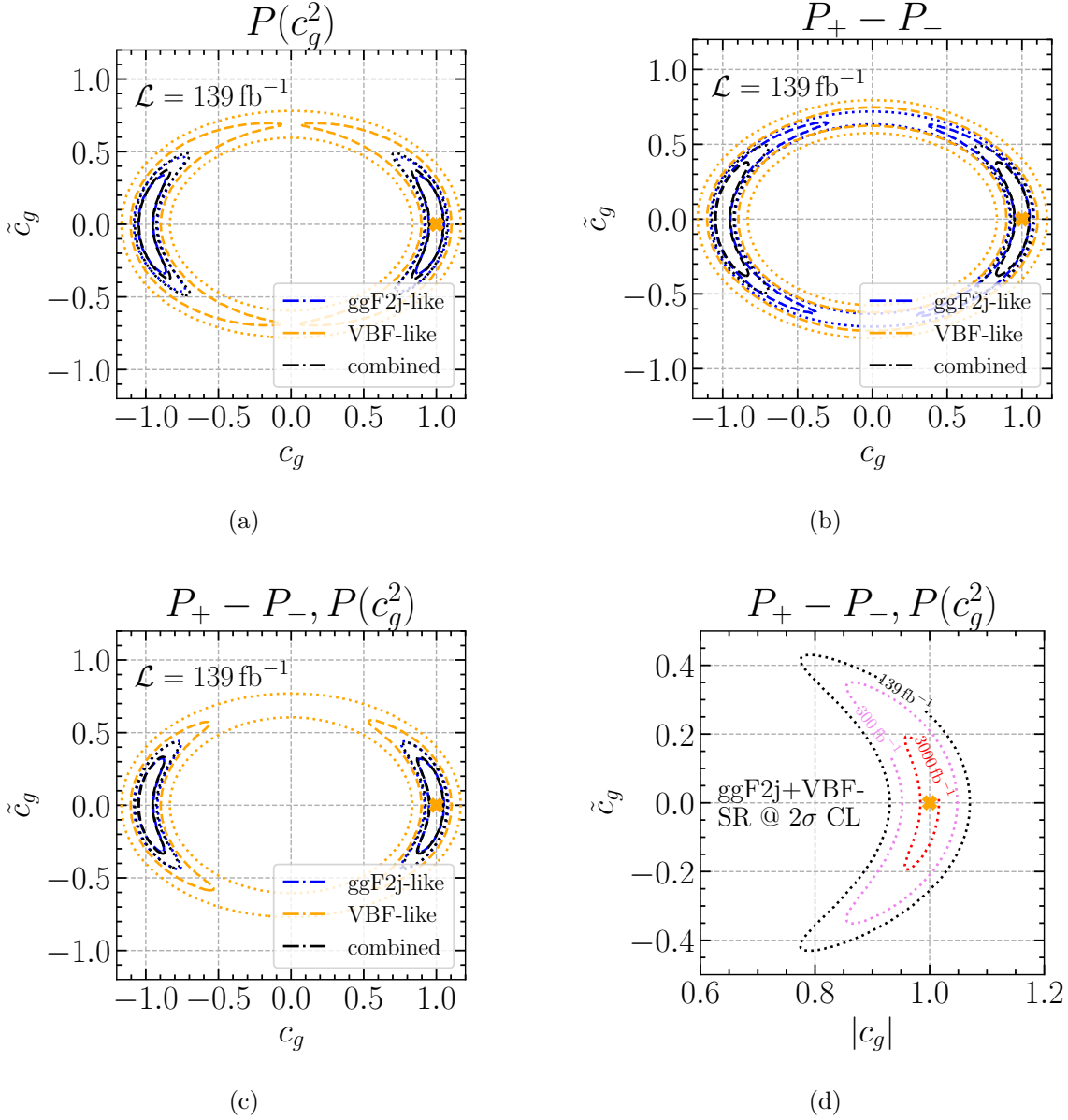


**Figure 10:** Comparison of the limits on the coupling modifiers in the ggF2j-, VBF- and combined SRs for the  $P(c_g^2)$  (a) and  $P_+ - P_-$  (b) observables, their combination (c) and projections to higher luminosities (d). The  $1\sigma$  regions are shown as dashed lines, while the dotted lines correspond to the  $2\sigma$  confidence levels. The SM is marked by an orange cross.

the  $\Delta\phi_{jj}$  distribution. As we have shown, these restrictions significantly lower the expected sensitivity. On the other hand, the limits derived here are also expected to degrade once systematic uncertainties are considered.

## 5.4 Highest-impact observables

Here, we evaluate the impact of the various observables used by the classifiers on the output of the  $\mathcal{CP}$  classifier. We evaluate this impact with the SHAP package [103], which explains the output in terms of Shapley values from cooperative game theory [104, 105]: Each classifier has a fixed "worth" determined from its separation power when all variables are used in the training. The Shapley value of one variable  $x_i$  is then determined by taking the sum over all possible subsets of the parameter space not containing  $x_i$  and evaluating the loss in worth compared to the full case. Taking every possible subspace into account guarantees that possible correlations between variables do not falsify the result. For more details, we refer to Ref. [106]. In the following, the Shapley values are referred to as SHAP values to meet the nomenclature of the SHAP package.

The SHAP plots are structured as follows:

- Individual variables are plotted against their SHAP value. A point at a high absolute SHAP value means that the variable had a large impact on deciding what label the event has been given by the classifier. The sign of the SHAP value determines which label was chosen, i.e., for the  $|\mathcal{M}_{\text{even}}|^2$  vs.  $|\mathcal{M}_{\text{odd}}|^2$  classifier, a positive sign signals that  $|\mathcal{M}_{\text{even}}|^2$  is more likely to be chosen.
- The color of the points represents the value of the variable itself. Red points stand for high values of the variable, while blue ones stand for low ones.
- The variables are ranked by the mean of the absolute SHAP value. Therefore, variables which have many events (displayed as bulks) deviating from zero are identified as the most important ones. Single points of variables that reach high absolute SHAP values are understood as outliers and only have a minor impact.

We first focus on the classifier separating the squared ggF2j terms in the respective signal regions in Fig. 11. In the ggF2j-SR (see Fig. 11(a)) the most important variables are  $p_T$  and  $E$  of the leading- $p_T$  jets, as well as their invariant mass, while the observables associated with the Higgs boson play a subordinate role. This picture is flipped in the VBF-SR (see Fig. 11(b)) where now  $p_T$  and  $E$  of the Higgs boson are the most important variables, followed by the jet kinematics. Note that the overall absolute SHAP values are relatively low compared to their spread indicating that no single observable drives the outcome of the classifiers. Instead, the full kinematic information is needed to separate between the squared ggF2j terms.

In the case of the interference classifiers (see Fig. 12),  $\Delta\phi_{jj}$  is by far the most important variable for both signal regions. As a  $\mathcal{CP}$ -odd observable by construction,  $\Delta\phi_{jj}$  is expected

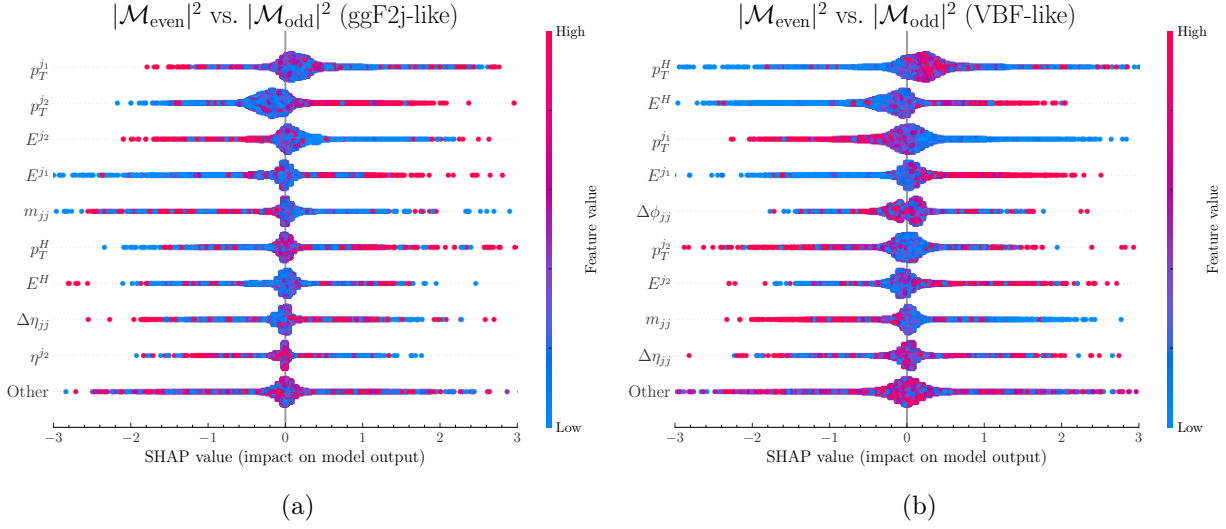


**Figure 11:** SHAP values for the variables used in classifiers separating the  $|\mathcal{M}_{\text{even}}|^2$  and  $|\mathcal{M}_{\text{odd}}|^2$  terms. The classifiers are trained in (a) the ggF2j-SR and (b) the VBF-SR. High absolute SHAP values indicate a strong influence on the classifier score. The color of individual points marks the value of the specific variable. The variables are ordered by taking the mean of the absolute SHAP value. All variables used in the training which are not shown in the plot are summed up and marked as “Others”.

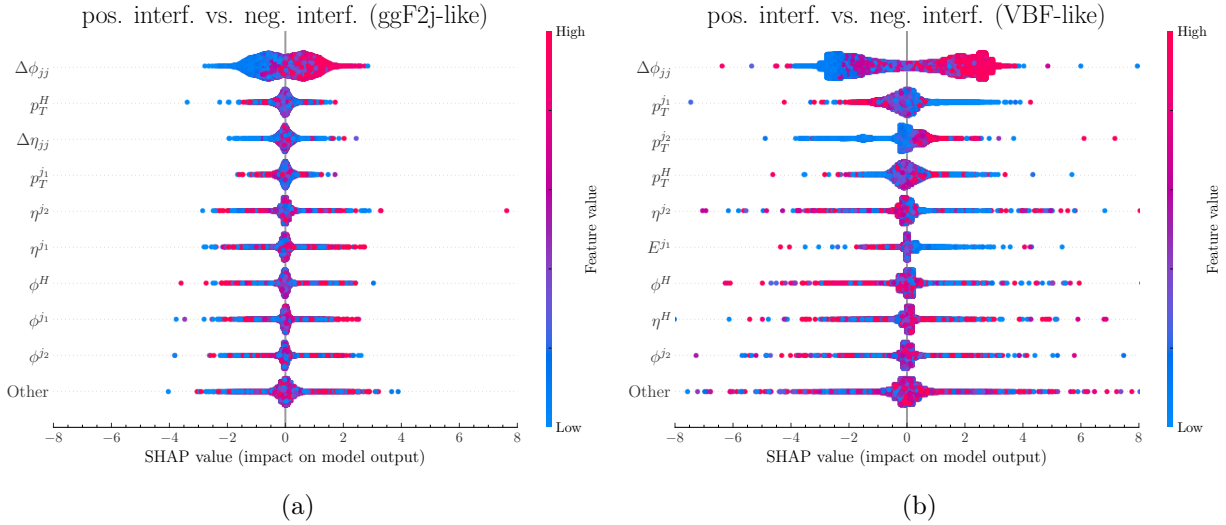


**Figure 12:** Same as Fig. 11, but the SHAP values for the classifiers separating the positive and negative interference terms are shown.

to give a good separation between the positive and negative parts of the interference. In the ggF2j-SR (Fig. 12(a)), other important variables are the  $p_T$  of the Higgs boson, as well as the pseudorapidity of the jets — in the form of the combination  $\Delta\eta_{jj}$  as well as  $\eta^{j1}$  and  $\eta^{j2}$  alone. For the VBF-SR (Fig. 12(b)), it should be noted that the mean of the  $\Delta\phi_{jj}$  distribution peaks at much higher SHAP values than in the ggF2j-SR. This is in agreement with the limits obtained in Section 5.2, where the limits from the classifier using the full event kinematics showed only a slight improvement over the limits from  $\Delta\phi_{jj}$  alone. The next two most sensitive variables are  $p_T^{j1}$  and  $p_T^{j2}$ . Our findings agree with Ref. [107], in which  $\mathcal{CP}$ -violating effects in the Higgs coupling to  $W$  bosons were studied with a different machine learning approach, identifying  $\Delta\phi_{jj}$ ,  $p_T^{j1}$  and  $p_T^{j2}$  as the three most sensitive observables for this coupling when using the product of all three variables.

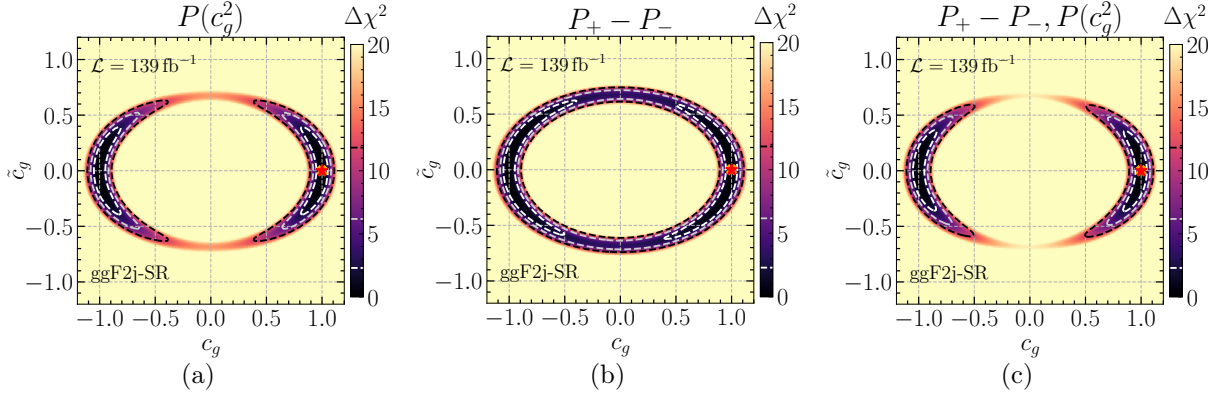
## 6 Disentangling $\mathcal{CP}$ violation in the $ggH$ and $HVV$ couplings

So far, we have concentrated on  $\mathcal{CP}$  violation in the Higgs–gluon interaction. However, BSM physics may affect multiple Higgs couplings at once. As discussed above, VBF production is the main background for investigations of ggF2j production. While, as mentioned in Section 1, a lot of effort has been put forward already to investigate the  $\mathcal{CP}$  structure of the Higgs couplings to massive vector bosons, we investigate in this section how the presence of  $\mathcal{CP}$  violation in the  $HVV$  couplings influence our limits on the Higgs–gluon coupling in the two signal regions.

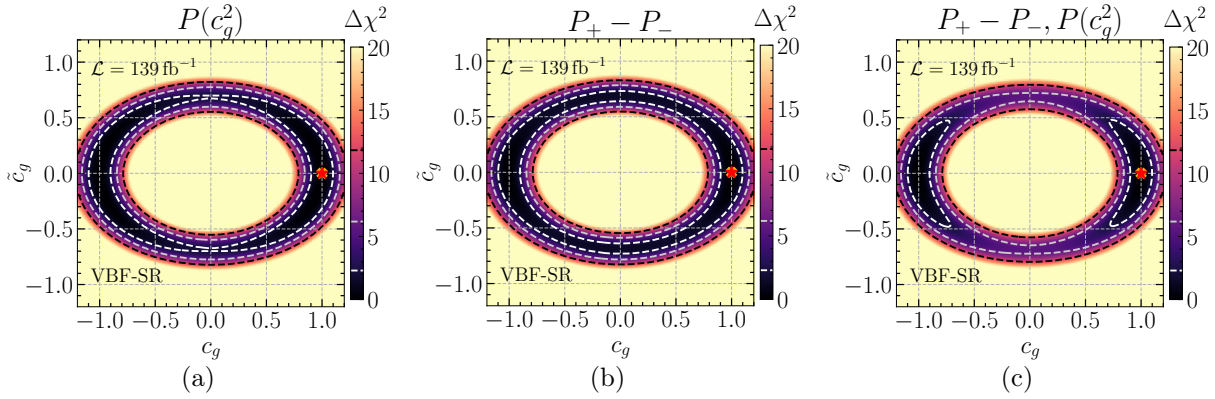
For this, we generate an additional data set for VBF production in the context of the SMEFT, where a non-zero value of the  $c_{\Phi\tilde{W}}$  Wilson coefficient introduces  $\mathcal{CP}$  violation in the Higgs coupling to  $W$  bosons (for details see Appendix A). This data set is added to the SM-like VBF data set which has been used for our analysis so far. To quantify the effects on our Higgs–gluon coupling limits, we do not re-train our classifiers, but directly build new observables based on the adjusted events.

Fig. 13 depicts the limits obtained in the ggF2j-SR when using the VBF data set with  $\mathcal{CP}$  violation. Compared to the limits in Fig. 8 in the same signal region, we obtain slightly weaker limits from the classifier trained on the  $|\mathcal{M}_{\text{even}}|^2$  and  $|\mathcal{M}_{\text{odd}}|^2$  terms. Now the  $1\sigma$  contour reaches  $|\tilde{c}_g| = 0.4$  instead of  $|\tilde{c}_g| = 0.35$ , as visible in Fig. 13(a). In contrast, we obtain slightly tighter constraints from the interference classifier in comparison to the results without  $\mathcal{CP}$  violation in the  $HVV$  interaction (Fig. 13(b)). This change is not significant enough to exclude smaller values of  $|\tilde{c}_g|$  or affect the combined limits of the two classifiers (see Fig. 13(c) and Fig. 8(d)) since these limits are mostly dominated by  $P(c_g^2)$ . Accordingly, they get slightly weaker as well compared to previous results, excluding  $|\tilde{c}_g| > 0.37$  compared to  $|\tilde{c}_g| > 0.32$  obtained in Section 5.1. In general, both the comparably low cross section of VBF compared to ggF2j, and the small number of VBF events surviving the ggF2j signal selection suppress any large changes in the limits. This makes the ggF2j-SR robust against





**Figure 13:** Same as Fig. 8, but the limits are shown for the case that  $\mathcal{CP}$  violation is present in VBF production.



**Figure 14:** Same as Fig. 9, but the limits are shown for the case that  $\mathcal{CP}$  violation is present in VBF production.

$\mathcal{CP}$  violation in the  $HVW$  coupling.

The limits based on the VBF-SR with  $\mathcal{CP}$  violation in the VBF data are plotted in Fig. 14. The limits obtained individually from the  $P(c_g^2)$  (Fig. 14(a)) or  $P_+ - P_-$  (Fig. 14(b)) observables do not differ significantly compared to the case of SM-like VBF production. We do, however, observe stronger limits for the combination of both classifiers when compared to the previous results in Section 5.2 (see Fig. 9). Here, the  $1\sigma$  limits from the combined classifier tighten noticeably from  $\tilde{c}_g \in [-0.58, 0.58]$  to  $\tilde{c}_g \in [-0.48, 0.48]$ .

The opposite effects on the limits in the two signal regions most likely stem from a “washout” of events. Since the classifiers were never trained to identify  $\mathcal{CP}$ -odd VBF events, a higher (lower) total number of VBF events are now identified as ggF2j-like (VBF-like) events. Therefore, this yields more (less) background events in the ggF2j-SR (VBF-SR), leading to the observed weakened (tightened) limits. We emphasize that consequently the interpretation of these results should be done carefully, as the “better“ constraints in the VBF-SR on  $c_g$  and  $\tilde{c}_g$  are faked from  $\mathcal{CP}$  violation in the  $HVW$  couplings.

Overall we conclude that additional  $\mathcal{CP}$  violation in the  $HVW$  coupling can have different

effects depending on the signal region. As expected, all effects are suppressed in the ggF2j-SR. However, a slight trend towards weaker limits stemming from the  $HVV$   $\mathcal{CP}$  violation can be identified. On the other hand, this additional  $\mathcal{CP}$  violation can lead to seemingly stronger limits in the VBF-SR. Together with the overall better limits in the ggF2j-SR, our findings consolidate the need for a dedicated signal region with ggF2j-like kinematics.

## 7 Limits on the $\mathcal{CP}$ structure of the top-Yukawa coupling

As discussed in Section 2.2, we normalized the coefficients of the effective Higgs–gluon interaction (see Eq. (1)) such that they directly correspond to the modifiers of the top-Yukawa coupling (see Eq. (2)) if no low-mass coloured BSM particles are present and if we neglect the contributions of the lighter quarks. Since experimental limits on coloured BSM particles are becoming increasingly strong [80–85], these particles can also only induce a small  $\mathcal{CP}$ -odd Higgs–gluon coupling. Taking as an example a coloured fermion with a mass of 1 TeV and a Yukawa-type coupling of  $\mathcal{O}(1)$  to the Higgs boson, we expect this fermion to contribute to the Higgs–gluon couplings at the  $\mathcal{O}(v^2/\Lambda^2) \sim 0.1$ .

Assuming that the contribution of coloured BSM particles is negligible, we can reinterpret our projected limits on the Higgs–gluon coupling as projected limits on the top-Yukawa coupling (by simply replacing  $c_g$  by  $c_t$  and  $\tilde{c}_g$  by  $\tilde{c}_t$ ). Our findings as well as a comparison to other approaches are summarized in Table 2 and described in detail in the following.

Our projected limits on the  $\mathcal{CP}$  mixing angle  $\alpha^{\text{Htt}} = \tan^{-1}(\tilde{c}_t/c_t)$  for a luminosity of  $139 \text{ fb}^{-1}$  result in

$$\alpha_{\text{ggF2j}}^{\text{Htt}} \in [-15^\circ, 15^\circ], \quad \alpha_{\text{VBF}}^{\text{Htt}} \in [-25^\circ, 25^\circ] \quad @ \text{ 68\% CL} \quad (5)$$

for the respective signal regions. Our result for the ggF2j-SR is stronger than existing experimental limits on  $\alpha^{\text{Htt}}$  based on ggF2j production —  $\alpha^{\text{Htt}} \in [-26^\circ, 26^\circ]$ , see Refs. [29, 30] — while our result in the VBF-SR is very similar. We, however, want to stress several differences between our approach and the one in Ref. [30] that make a direct comparison of the results difficult. In contrast to our study, the authors worked in the  $H \rightarrow \tau\tau$  decay channel and took systematic uncertainties as well as bottom-quark contributions to the Higgs–gluon loop into account (see also discussion at the end of Section 5.3).

In addition to limits on  $\alpha^{\text{Htt}}$  based on ggF2j production, our projected bound is also tighter than existing experimental limits focusing on top-associated Higgs production ( $\alpha^{\text{Htt}} \in [-35^\circ, 35^\circ]$  at 68% CL) [30, 35–39].

Moreover, our projected limits are stronger than the results of recent global fits [20, 66]. Besides many other total rate and simplified template cross-section measurements, these fits take into account total rate information from Higgs production via gluon fusion and the Higgs decay to two photons, which are very sensitive, but model-dependent constraints.

To provide an up-to-date comparison, we have updated the fits performed in Refs. [20, 66] using the new `HiggsSignals` which is part of `HiggsTools` and contains additional recent



process/ SR	our work		literature		
	68% CL	95% CL	68% CL	95% CL	Ref.
$gg \rightarrow Hjj$ : ggF2j-SR	15°	25°	–	–	–
$gg \rightarrow Hjj$ : VBF-SR	25°	–	26°	–	[30]
$t\bar{t}H$	–	–	35°	43°	[36]
global fit	21°	28°	see text and Refs. [20, 66]		

**Table 2:** Upper limits on  $|\alpha^{\text{H}t\bar{t}}|$  at the 68% and 95% CL obtained from the different signal regions (SR) from our work compared to the literature. See text regarding caveats of the comparison of these limits.

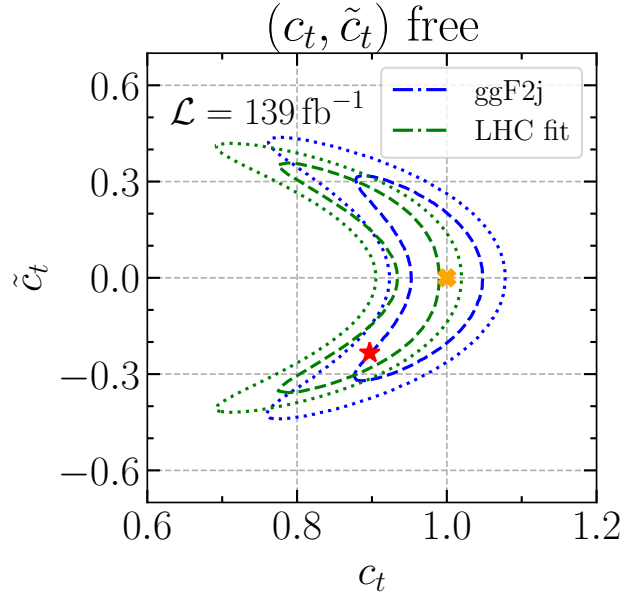


**Figure 15:** Comparison of the projected combined ggF2j limits (blue) to the current global limits from LHC data (green). Shown are the  $1\sigma$  (dashed) and  $2\sigma$  regions (dotted) in both cases. The SM is marked by an orange cross and the BF point of the LHC data by a red star.

experimental results [108–110].<sup>5</sup> The result is shown in the  $(c_t, \tilde{c}_t)$  parameter plane in Fig. 15. The blue contours depict the limits from our ggF2j analysis, and the green ones are based on the global fit to existing experimental results. As discussed in detail in Ref. [66], the fit constraints are dominated by total rate measurements of Higgs production via gluon fusion and the Higgs decay to two photons.<sup>6</sup> By exploiting the kinematic information, our projected limits are less model-dependent and (slightly) stronger.

## 8 Conclusions

The  $\mathcal{CP}$  nature of the Higgs boson is among the few Higgs properties which are still only loosely constrained. One coupling, which is especially important for LHC physics, is the Higgs–gluon interaction — facilitated at the loop level. The  $\mathcal{CP}$  structure of this interaction can be probed via Higgs production in association with two jets (ggF2j).

In this work, we studied how the information about the  $\mathcal{CP}$  structure of the Higgs–gluon interaction can be best extracted. Focusing on the Higgs decay to two photons, we first trained a classifier to define a ggF2j-enriched signal region differentiating it from VBF and  $VH$  production as the relevant backgrounds. In order to fully exploit the quark-initiated ggF2j channel, which is kinematically very similar to VBF production, we also defined a VBF-enriched signal region.

For both SRs, we trained two classifiers to separate the different contributions to the squared ggF2j amplitude: the square of the  $\mathcal{CP}$ -even amplitude, the square of the  $\mathcal{CP}$ -odd amplitude, and the interference contribution. Out of these classifiers, we constructed one  $\mathcal{CP}$ -even and one  $\mathcal{CP}$ -odd observable. Based on the distributions for these observables, we derived expected upper limits. These constrain the  $\mathcal{CP}$ -odd Higgs–gluon coupling modifier to  $|\tilde{c}_g| \leq \{0.35, 0.28, 0.15\}$  at the  $2\sigma$  level for integrated luminosities of  $\{139 \text{ fb}^{-1}, 300 \text{ fb}^{-1}, 3000 \text{ fb}^{-1}\}$ , respectively. We found these to significantly outperform limits based only on the difference in the azimuthal angle of the two leading jets, which is an observable commonly employed in the literature. Moreover, the ggF2j-SR has a significantly higher sensitivity than the VBF-SR, which is expected by the higher number of ggF2j events. These results suggest that significant improvements in current experimental limits are possible with well-established techniques.

We note that our limits could be further improved by including other Higgs decay channels and removing the cut on the Higgs transverse momentum. Moreover, advanced analysis techniques like e.g. the matrix-element approach [54, 112–120] or machine-learning-based inference [121–125] could be used. We leave such improvements for future work.

In addition, we used interpretable machine learning (in the form of SHAP values) to investigate which observables have the highest impact on the classifications. While the az-

---

<sup>5</sup>We are using version 1.1 of the HiggsSignals data set.

<sup>6</sup>The observed shift of the  $1\sigma$  and  $2\sigma$  regions to lower values of  $c_t$  is caused by recent experimental measurements of top-associated Higgs production and Higgs production via gluon fusion with a lower rate than expected in the SM [33, 111].

imuthal angle of the two leading jets is by far the most important observable for separating the interference term from the squared terms, also other momenta like the transverse momenta of the jets and the Higgs boson play a sizeable role. For separating the squared  $\mathcal{CP}$ -even and  $\mathcal{CP}$ -odd amplitudes, the transverse momenta are most decisive.

We also investigated the model dependence of our limits. In particular, we checked whether  $\mathcal{CP}$ -violating couplings in the VBF channel could mimic a  $\mathcal{CP}$ -violating Higgs–gluon interaction in our analysis. Our results show that our analysis — in particular the ggF2j-SR — is very robust to such a situation and therefore allows to disentangle  $\mathcal{CP}$ -violating Higgs couplings to massive vector bosons and gluons.

Finally, we reinterpreted our expected limits in terms of limits on the  $\mathcal{CP}$  character of the top-Yukawa coupling. This reinterpretation relies on the assumption that no coloured BSM particles contribute sizeably to Higgs production to gluon fusion, which is motivated by the current limits from direct searches for such particles. The projected limits on the  $\mathcal{CP}$  structure of the top-Yukawa coupling from our reinterpretation are stronger than limits based on existing dedicated analyses of the top-Yukawa coupling based either on investigations of top-associated Higgs production or on global fits to Higgs precision measurements using the Run-2 data of the LHC. Both for the current data and for future runs of the LHC, this demonstrates the large potential of ggF2j production as a precision probe of the  $\mathcal{CP}$  nature of the Higgs boson.

## Acknowledgements

We thank Alberto Carnelli, Frederic Deliot, Christian Grefe, Andrei Gritsan, Lena Herrmann, Anastasia Kotsoskechagia, Andrew Pilkington, Tilman Plehn, Matthias Saimpert and Laurent Schoeffel for useful discussions. HB acknowledges support from the Alexander von Humboldt Foundation. EF and MM acknowledge support by the Deutsche Forschungsgemeinschaft (DFG, German Research Foundation) under Germany’s Excellence Strategy — EXC-2123 “QuantumFrontiers” — 390837967.

## A Details of the event generation

The model file used for the event generation is a custom UFO model file [96, 97] which only contains the terms in Eq. (1), as well as an effective Higgs-photon coupling. The  $H\gamma\gamma$  coupling is assumed to be SM-like throughout this study. It is implemented as an effective coupling to enable the generation of the ggF2j process at the tree level. With  $\mathbf{G} \equiv g$ ,  $\mathbf{GA} \equiv \gamma$ ,  $\mathbf{H} \equiv \text{scalar}$  and  $\mathbf{A} \equiv \text{pseudoscalar}$ , there are four effective couplings:  $\mathbf{QGGH}$ ,  $\mathbf{QGGA}$ ,  $\mathbf{QGAGAH}$  and  $\mathbf{QGAGAA}$  that are used to generate specific parts of the amplitude. Setting  $\mathbf{QGGH}==1$ ,  $\mathbf{QGAGAH}==1$  ( $\mathbf{QGGA}==1$ ,  $\mathbf{QGAGAA}==1$ ) implies the effective interaction of a scalar (pseudoscalar) Higgs boson with exactly one pair of gluons and one pair of photons. The parameters can be set during the event generation, as seen in the following. All events are generated at leading

order and are scaled to NLO by flat K-factors from Ref. [47].

The syntax for the event generation is “generate p p > a a j j QGGH==1 QGAGAH==1 QED=4 QCD=4” for the  $|\mathcal{M}_{\text{even}}|^2$  term in ggF2j, where the restrictions on the QED and QCD magnitude are set to exclude di-Higgs production. The interference and  $|\mathcal{M}_{\text{odd}}|^2$  terms are created by replacing “QGGH==1” by “QGGH^2==1 QGGA^2==1” and “QGGA==1”, respectively. For the background processes, the effective Higgs-gluon coupling has been disabled in the model file. The VBF background is generated via “generate p p > a a j j \$\$ w+ w- z QGAGAH==1” where heavy vector bosons are forbidden to appear in the s-channel to exclude contributions from the  $VH$  background. The latter is in turn generated via “generate p p > z > a a j j QGAGAH==1; add process p p > w+ > a a j j QGAGAH==1; add process p p > w- > a a j j QGAGAH==1”.

An additional data set introducing  $\mathcal{CP}$  violation in the VBF channel, used for the analysis in Section 6, is generated using the SMEFTsim 3.0 package [126]. Specifically, the U35 model is used in the  $m_W$ -scheme and we set  $c_{\phi\tilde{W}} = 1 \text{ TeV}^{-1}$  as the only non-zero BSM parameter of the model. Events are then generated via “generate p p > a a j j \$\$ w+ w- z /a QCD=0 NP=1 NP^2==1” and we apply an additional diagram filter to ensure that only VBF events are generated.

## B Distributions of kinematic variables

Fig. 16 shows the distributions of all variables used in the training of the classifiers (see Section 4.1), separately for the three different  $\mathcal{CP}$  contributions to the squared ggF2j amplitude. These include as low-level observables the energy  $E$ , transverse momentum  $p_T$  and pseudo-rapidity  $\eta$  of the reconstructed final state particles, as well as some high-level observables. An exception to this is the azimuthal angle  $\phi$  of the aforementioned objects as this does not exhibit any separation between the three contributions due to the rotational invariance of the production process.

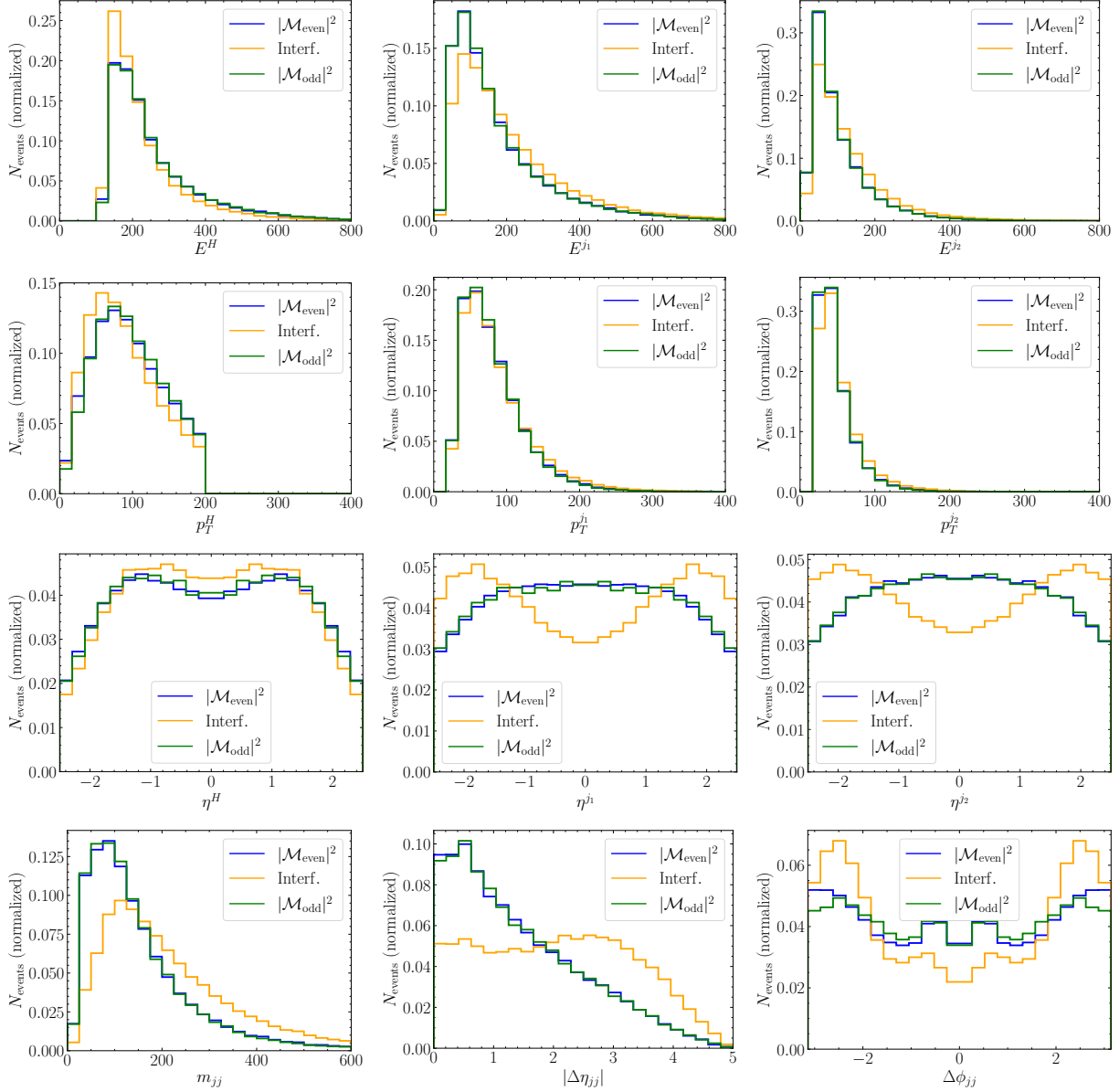


**Figure 16:** Distributions of the energy (first row),  $p_T$  (second row) and  $\eta$  (third row) of the Higgs boson (left column), as well as the jets leading (middle column) and sub-leading (right column) in  $p_T$ . The last row shows distributions of high-level observables, namely the invariant mass of the di-jet system  $m_{jj}$  (left), as well as the difference in pseudorapidity  $\Delta\eta_{jj}$  (middle) and azimuthal angle  $\Delta\phi_{jj}$  (right) of the two jets. All distributions are split up into the  $|\mathcal{M}_{\text{even}}|^2$  (blue), interference (orange) and  $|\mathcal{M}_{\text{odd}}|^2$  (green) contributions to the total ggF2j cross section.

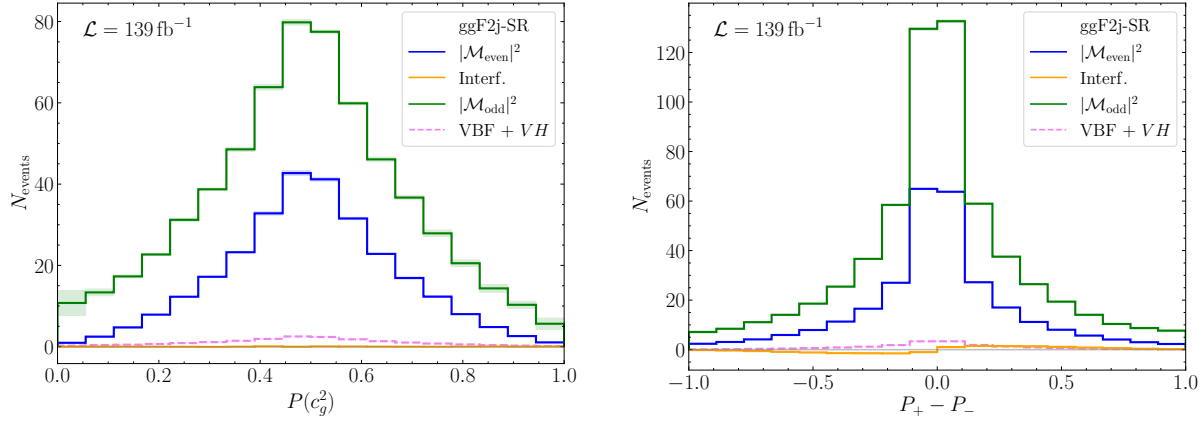


**Figure 17:** Distributions of the two  $\mathcal{CP}$  discriminants for the mean of 100 trained classifiers in the ggF2j-like kinematic region.

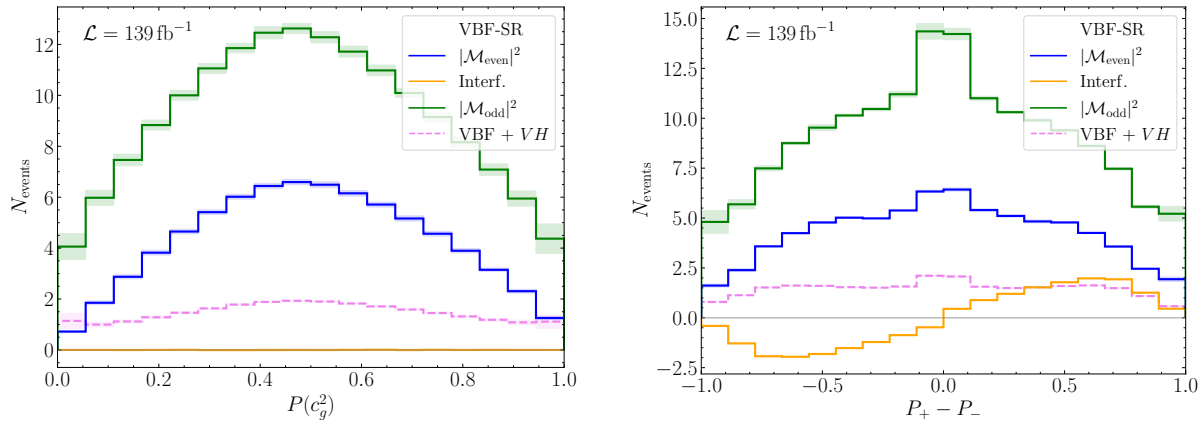


**Figure 18:** Distributions of the two  $\mathcal{CP}$  discriminants for the mean of 100 trained classifiers in the VBF-like kinematic region.

## C Training uncertainty

In Fig. 17, the classifier outputs for the two  $\mathcal{CP}$  discriminants in the ggF2j-like kinematic region are shown as the mean of 100 individual training processes, with the standard deviation in each bin plotted as a shaded region. This allows us to estimate the uncertainty due to the classifier training. We observe that the largest uncertainties come from bins close to 0 and 1 in the  $P(c_g^2)$  classifier. For the  $P_+ - P_-$  classifier, the uncertainty associated with the training process is negligible. In the VBF-like region (see Fig. 18), the visible statistical fluctuations in the  $|\mathcal{M}_{\text{even}}|^2$  and  $|\mathcal{M}_{\text{odd}}|^2$  contributions arise due to the comparably low number of ggF2j events in this kinematic region.

It should be noted that, in the present study, the uncertainty associated with the training process does not result in an uncertainty on the extraction of the Higgs–gluon couplings. Each trained classifier represents a slightly different observable. Consequently, the best-

performing classifier can be chosen without introducing any further uncertainty in the final limits on the Higgs–gluon coupling.

## D Likelihood evaluation

As mentioned above, the output of the  $\mathcal{CP}$  classifiers is used to construct different observables. These observables are represented as histograms filled by all events from the respective test data set. Since each bin corresponds to a number of events, which follow a Poisson distribution, the histograms can be used to construct a likelihood

$$L_X = \frac{e^{-\lambda_X} \lambda_X^n}{n!} . \quad (6)$$

Here,  $\lambda_X$  is the expected number of events for a specific  $\mathcal{CP}$  hypothesis, while  $n$  corresponds to the observed number of events. We set  $n = \lambda_{\text{SM}}$ , which corresponds to a perfect agreement of the data with the SM hypothesis, in order to construct limits on the Higgs–gluon coupling.

These limits are calculated using a binned likelihood ratio

$$\begin{aligned} t &= -2 \ln \left( \frac{L_{\text{tot}}}{L_{\text{SM}}} \right) = -2 \ln \left( \prod_i \frac{e^{-\lambda_{i,\text{tot}}} \lambda_{i,\text{tot}}^{n_i}}{e^{-\lambda_{i,\text{SM}}} \lambda_{i,\text{SM}}^{n_i}} \right) \\ &= -2 \sum_i \left[ \lambda_{\text{SM}}^i \cdot \ln \left( \frac{\lambda_{\text{tot}}^i}{\lambda_{\text{SM}}^i} \right) - \lambda_{\text{tot}}^i + \lambda_{\text{SM}}^i \right] , \end{aligned} \quad (7)$$

where  $t$  is the test statistic and the sum runs over all bins  $i$ .  $\lambda_{\text{SM}}^i = \lambda_{\text{E1}}^i + \lambda_{\text{BG}}^i$  is the expected SM distribution including ggF2j with  $c_g = 1, \tilde{c}_g = 0$  and the BG processes, while  $\lambda_{\text{tot}}^i = c_g^2 \lambda_{\text{E1}}^i + c_g \tilde{c}_g \lambda_{\text{O}}^i + \tilde{c}_g^2 \lambda_{\text{E2}}^i + \lambda_{\text{BG}}^i$  is the total bin value in the BSM case where  $c_g$  and  $\tilde{c}_g$  can be varied. Following Wilks’ theorem [127], we assume that  $t$  follows a  $\chi^2$ -distribution and can, therefore, be used to construct confidence intervals.

## References

- [1] G. Aad et al. “Observation of a new particle in the search for the Standard Model Higgs boson with the ATLAS detector at the LHC”. In: *Phys. Lett.* B716 (2012), pp. 1–29. DOI: [10.1016/j.physletb.2012.08.020](https://doi.org/10.1016/j.physletb.2012.08.020). arXiv: [1207.7214](https://arxiv.org/abs/1207.7214) [hep-ex].
- [2] S. Chatrchyan et al. “Observation of a new boson at a mass of 125 GeV with the CMS experiment at the LHC”. In: *Phys. Lett.* B716 (2012), pp. 30–61. DOI: [10.1016/j.physletb.2012.08.021](https://doi.org/10.1016/j.physletb.2012.08.021). arXiv: [1207.7235](https://arxiv.org/abs/1207.7235) [hep-ex].
- [3] “A detailed map of Higgs boson interactions by the ATLAS experiment ten years after the discovery”. In: *Nature* 607.7917 (2022). [Erratum: *Nature* 612, E24 (2022)], pp. 52–59. DOI: [10.1038/s41586-022-04893-w](https://doi.org/10.1038/s41586-022-04893-w). arXiv: [2207.00092](https://arxiv.org/abs/2207.00092) [hep-ex].
- [4] A. Tumasyan et al. “A portrait of the Higgs boson by the CMS experiment ten years after the discovery”. In: *Nature* 607.7917 (2022), pp. 60–68. DOI: [10.1038/s41586-022-04892-x](https://doi.org/10.1038/s41586-022-04892-x). arXiv: [2207.00043](https://arxiv.org/abs/2207.00043) [hep-ex].
- [5] M. B. Gavela et al. “Standard model CP violation and baryon asymmetry”. In: *Mod. Phys. Lett. A* 9 (1994), pp. 795–810. DOI: [10.1142/S0217732394000629](https://doi.org/10.1142/S0217732394000629). arXiv: [hep-ph/9312215](https://arxiv.org/abs/hep-ph/9312215).
- [6] P. Huet and E. Sather. “Electroweak baryogenesis and standard model CP violation”. In: *Phys. Rev. D* 51 (1995), pp. 379–394. DOI: [10.1103/PhysRevD.51.379](https://doi.org/10.1103/PhysRevD.51.379). arXiv: [hep-ph/9404302](https://arxiv.org/abs/hep-ph/9404302).
- [7] V. Khachatryan et al. “Constraints on the spin-parity and anomalous HVV couplings of the Higgs boson in proton collisions at 7 and 8 TeV”. In: *Phys. Rev. D* 92.1 (2015), p. 012004. DOI: [10.1103/PhysRevD.92.012004](https://doi.org/10.1103/PhysRevD.92.012004). arXiv: [1411.3441](https://arxiv.org/abs/1411.3441) [hep-ex].
- [8] G. Aad et al. “Study of the spin and parity of the Higgs boson in diboson decays with the ATLAS detector”. In: *Eur. Phys. J. C* 75.10 (2015). [Erratum: *Eur.Phys.J.C* 76, 152 (2016)], p. 476. DOI: [10.1140/epjc/s10052-015-3685-1](https://doi.org/10.1140/epjc/s10052-015-3685-1). arXiv: [1506.05669](https://arxiv.org/abs/1506.05669) [hep-ex].
- [9] M. Pospelov and A. Ritz. “Electric dipole moments as probes of new physics”. In: *Annals Phys.* 318 (2005), pp. 119–169. DOI: [10.1016/j.aop.2005.04.002](https://doi.org/10.1016/j.aop.2005.04.002). arXiv: [hep-ph/0504231](https://arxiv.org/abs/hep-ph/0504231).
- [10] T. Chupp et al. “Electric dipole moments of atoms, molecules, nuclei, and particles”. In: *Rev. Mod. Phys.* 91.1 (2019), p. 015001. DOI: [10.1103/RevModPhys.91.015001](https://doi.org/10.1103/RevModPhys.91.015001). arXiv: [1710.02504](https://arxiv.org/abs/1710.02504) [physics.atom-ph].
- [11] V. Andreev et al. “Improved limit on the electric dipole moment of the electron”. In: *Nature* 562.7727 (2018), pp. 355–360. DOI: [10.1038/s41586-018-0599-8](https://doi.org/10.1038/s41586-018-0599-8).
- [12] T. S. Roussy et al. “An improved bound on the electron’s electric dipole moment”. In: *Science* 381.6653 (2023), adg4084. DOI: [10.1126/science.adg4084](https://doi.org/10.1126/science.adg4084). arXiv: [2212.11841](https://arxiv.org/abs/2212.11841) [physics.atom-ph].
- [13] G. Pignol and P. Schmidt-Wellenburg. “The search for the neutron electric dipole moment at PSI”. In: *SciPost Phys. Proc.* 5 (2021), p. 027. DOI: [10.21468/SciPostPhys/nProc.5.027](https://doi.org/10.21468/SciPostPhys/nProc.5.027). arXiv: [2103.01898](https://arxiv.org/abs/2103.01898) [hep-ex].



- [14] B. Graner et al. “Reduced Limit on the Permanent Electric Dipole Moment of  $^{199}\text{Hg}$ ”. In: *Phys. Rev. Lett.* 116 (16 Apr. 2016), p. 161601. DOI: [10.1103/PhysRevLett.116.161601](https://doi.org/10.1103/PhysRevLett.116.161601). URL: <https://link.aps.org/doi/10.1103/PhysRevLett.116.161601>.
- [15] J. Brod, U. Haisch, and J. Zupan. “Constraints on CP-violating Higgs couplings to the third generation”. In: *JHEP* 11 (2013), p. 180. DOI: [10.1007/JHEP11\(2013\)180](https://doi.org/10.1007/JHEP11(2013)180). arXiv: [1310.1385](https://arxiv.org/abs/1310.1385) [[hep-ph](#)].
- [16] J. Brod and E. Stamou. “Electric dipole moment constraints on CP-violating heavy-quark Yukawas at next-to-leading order”. In: *JHEP* 07 (2021), p. 080. DOI: [10.1007/JHEP07\(2021\)080](https://doi.org/10.1007/JHEP07(2021)080). arXiv: [1810.12303](https://arxiv.org/abs/1810.12303) [[hep-ph](#)].
- [17] E. Fuchs et al. “ $CP$  violation from  $\tau$ ,  $t$  and  $b$  dimension-6 Yukawa couplings - interplay of baryogenesis, EDM and Higgs physics”. In: *JHEP* 05 (2020), p. 056. DOI: [10.1007/JHEP05\(2020\)056](https://doi.org/10.1007/JHEP05(2020)056). arXiv: [2003.00099](https://arxiv.org/abs/2003.00099) [[hep-ph](#)].
- [18] J. Brod et al. “Global constraints on Yukawa operators in the standard model effective theory”. In: *JHEP* 08 (2022), p. 294. DOI: [10.1007/JHEP08\(2022\)294](https://doi.org/10.1007/JHEP08(2022)294). arXiv: [2203.03736](https://arxiv.org/abs/2203.03736) [[hep-ph](#)].
- [19] J. Brod, Z. Polonsky, and E. Stamou. “A Precise Electron EDM Constraint on CP-odd Heavy-Quark Yukawas”. In: (June 2023). arXiv: [2306.12478](https://arxiv.org/abs/2306.12478) [[hep-ph](#)].
- [20] H. Bahl et al. “Constraining the  $CP$  structure of Higgs-fermion couplings with a global LHC fit, the electron EDM and baryogenesis”. In: *Eur. Phys. J. C* 82.7 (2022), p. 604. DOI: [10.1140/epjc/s10052-022-10528-1](https://doi.org/10.1140/epjc/s10052-022-10528-1). arXiv: [2202.11753](https://arxiv.org/abs/2202.11753) [[hep-ph](#)].
- [21] G. Aad et al. “Search for the Higgs boson decays  $H \rightarrow ee$  and  $H \rightarrow e\mu$  in  $pp$  collisions at  $\sqrt{s} = 13$  TeV with the ATLAS detector”. In: *Phys. Lett. B* 801 (2020), p. 135148. DOI: [10.1016/j.physletb.2019.135148](https://doi.org/10.1016/j.physletb.2019.135148). arXiv: [1909.10235](https://arxiv.org/abs/1909.10235) [[hep-ex](#)].
- [22] Y. Soreq, H. X. Zhu, and J. Zupan. “Light quark Yukawa couplings from Higgs kinematics”. In: *JHEP* 12 (2016), p. 045. DOI: [10.1007/JHEP12\(2016\)045](https://doi.org/10.1007/JHEP12(2016)045). arXiv: [1606.09621](https://arxiv.org/abs/1606.09621) [[hep-ph](#)].
- [23] J. Brehmer et al. “Better Higgs-CP Tests Through Information Geometry”. In: *Phys. Rev. D* 97.9 (2018), p. 095017. DOI: [10.1103/PhysRevD.97.095017](https://doi.org/10.1103/PhysRevD.97.095017). arXiv: [1712.02350](https://arxiv.org/abs/1712.02350) [[hep-ph](#)].
- [24] G. Aad et al. “Test of CP Invariance in vector-boson fusion production of the Higgs boson using the Optimal Observable method in the ditau decay channel with the ATLAS detector”. In: *Eur. Phys. J. C* 76.12 (2016), p. 658. DOI: [10.1140/epjc/s10052-016-4499-5](https://doi.org/10.1140/epjc/s10052-016-4499-5). arXiv: [1602.04516](https://arxiv.org/abs/1602.04516) [[hep-ex](#)].
- [25] A. M. Sirunyan et al. “Constraints on anomalous Higgs boson couplings using production and decay information in the four-lepton final state”. In: *Phys. Lett. B* 775 (2017), pp. 1–24. DOI: [10.1016/j.physletb.2017.10.021](https://doi.org/10.1016/j.physletb.2017.10.021). arXiv: [1707.00541](https://arxiv.org/abs/1707.00541) [[hep-ex](#)].
- [26] A. M. Sirunyan et al. “Constraints on anomalous  $HVV$  couplings from the production of Higgs bosons decaying to  $\tau$  lepton pairs”. In: *Phys. Rev. D* 100.11 (2019), p. 112002. DOI: [10.1103/PhysRevD.100.112002](https://doi.org/10.1103/PhysRevD.100.112002). arXiv: [1903.06973](https://arxiv.org/abs/1903.06973) [[hep-ex](#)].

- [27] A. M. Sirunyan et al. “Measurements of the Higgs boson width and anomalous  $HVV$  couplings from on-shell and off-shell production in the four-lepton final state”. In: *Phys. Rev. D* 99.11 (2019), p. 112003. DOI: [10.1103/PhysRevD.99.112003](https://doi.org/10.1103/PhysRevD.99.112003). arXiv: [1901.00174](https://arxiv.org/abs/1901.00174) [hep-ex].
- [28] G. Aad et al. “Test of CP invariance in vector-boson fusion production of the Higgs boson in the  $H \rightarrow \tau\tau$  channel in proton–proton collisions at  $s=13\text{TeV}$  with the ATLAS detector”. In: *Phys. Lett. B* 805 (2020), p. 135426. DOI: [10.1016/j.physletb.2020.135426](https://doi.org/10.1016/j.physletb.2020.135426). arXiv: [2002.05315](https://arxiv.org/abs/2002.05315) [hep-ex].
- [29] G. Aad et al. “Constraints on Higgs boson properties using  $WW^*(\rightarrow e\nu\mu\nu)jj$  production in  $36.1\text{fb}^{-1}$  of  $\sqrt{s} = 13\text{TeV}$  pp collisions with the ATLAS detector”. In: *Eur. Phys. J. C* 82.7 (2022), p. 622. DOI: [10.1140/epjc/s10052-022-10366-1](https://doi.org/10.1140/epjc/s10052-022-10366-1). arXiv: [2109.13808](https://arxiv.org/abs/2109.13808) [hep-ex].
- [30] A. Tumasyan et al. “Constraints on anomalous Higgs boson couplings to vector bosons and fermions from the production of Higgs bosons using the  $\tau\tau$  final state”. In: *Phys. Rev. D* 108.3 (2023), p. 032013. DOI: [10.1103/PhysRevD.108.032013](https://doi.org/10.1103/PhysRevD.108.032013). arXiv: [2205.05120](https://arxiv.org/abs/2205.05120) [hep-ex].
- [31] G. Aad et al. “Test of CP Invariance in Higgs Boson Vector-Boson-Fusion Production Using the  $H \rightarrow \gamma\gamma$  Channel with the ATLAS Detector”. In: *Phys. Rev. Lett.* 131.6 (2023), p. 061802. DOI: [10.1103/PhysRevLett.131.061802](https://doi.org/10.1103/PhysRevLett.131.061802). arXiv: [2208.02338](https://arxiv.org/abs/2208.02338) [hep-ex].
- [32] G. Aad et al. “Test of CP-invariance of the Higgs boson in vector-boson fusion production and its decay into four leptons”. In: (Apr. 2023). arXiv: [2304.09612](https://arxiv.org/abs/2304.09612) [hep-ex].
- [33] A. Tumasyan et al. “Analysis of the  $CP$  structure of the Yukawa coupling between the Higgs boson and  $\tau$  leptons in proton-proton collisions at  $\sqrt{s} = 13\text{TeV}$ ”. In: *JHEP* 06 (2022), p. 012. DOI: [10.1007/JHEP06\(2022\)012](https://doi.org/10.1007/JHEP06(2022)012). arXiv: [2110.04836](https://arxiv.org/abs/2110.04836) [hep-ex].
- [34] G. Aad et al. “Measurement of the CP properties of Higgs boson interactions with  $\tau$ -leptons with the ATLAS detector”. In: *Eur. Phys. J. C* 83.7 (2023), p. 563. DOI: [10.1140/epjc/s10052-023-11583-y](https://doi.org/10.1140/epjc/s10052-023-11583-y). arXiv: [2212.05833](https://arxiv.org/abs/2212.05833) [hep-ex].
- [35] A. M. Sirunyan et al. “Measurements of  $t\bar{t}H$  Production and the CP Structure of the Yukawa Interaction between the Higgs Boson and Top Quark in the Diphoton Decay Channel”. In: *Phys. Rev. Lett.* 125.6 (2020), p. 061801. DOI: [10.1103/PhysRevLett.125.061801](https://doi.org/10.1103/PhysRevLett.125.061801). arXiv: [2003.10866](https://arxiv.org/abs/2003.10866) [hep-ex].
- [36] G. Aad et al. “ $CP$  Properties of Higgs Boson Interactions with Top Quarks in the  $t\bar{t}H$  and  $tH$  Processes Using  $H \rightarrow \gamma\gamma$  with the ATLAS Detector”. In: *Phys. Rev. Lett.* 125.6 (2020), p. 061802. DOI: [10.1103/PhysRevLett.125.061802](https://doi.org/10.1103/PhysRevLett.125.061802). arXiv: [2004.04545](https://arxiv.org/abs/2004.04545) [hep-ex].
- [37] A. M. Sirunyan et al. “Constraints on anomalous Higgs boson couplings to vector bosons and fermions in its production and decay using the four-lepton final state”. In: *Phys. Rev. D* 104.5 (2021), p. 052004. DOI: [10.1103/PhysRevD.104.052004](https://doi.org/10.1103/PhysRevD.104.052004). arXiv: [2104.12152](https://arxiv.org/abs/2104.12152) [hep-ex].

- [38] A. Tumasyan et al. “Search for  $CP$  violation in  $t\bar{t}H$  and  $tH$  production in multilepton channels in proton-proton collisions at  $\sqrt{s} = 13$  TeV”. In: *JHEP* 07 (2023), p. 092. DOI: [10.1007/JHEP07\(2023\)092](https://doi.org/10.1007/JHEP07(2023)092). arXiv: [2208.02686](https://arxiv.org/abs/2208.02686) [[hep-ex](#)].
- [39] ATLAS Collaboration. “Probing the  $CP$  nature of the top-Higgs Yukawa coupling in  $t\bar{t}H$  and  $tH$  events with  $H \rightarrow b\bar{b}$  decays using the ATLAS detector at the LHC”. In: (Mar. 2023). arXiv: [2303.05974](https://arxiv.org/abs/2303.05974) [[hep-ex](#)].
- [40] G. Aad et al. “Observation of four-top-quark production in the multilepton final state with the ATLAS detector”. In: *Eur. Phys. J. C* 83.6 (2023), p. 496. DOI: [10.1140/epjc/s10052-023-11573-0](https://doi.org/10.1140/epjc/s10052-023-11573-0). arXiv: [2303.15061](https://arxiv.org/abs/2303.15061) [[hep-ex](#)].
- [41] J. F. Gunion and X.-G. He. “Determining the CP nature of a neutral Higgs boson at the LHC”. In: *Phys. Rev. Lett.* 76 (1996), pp. 4468–4471. DOI: [10.1103/PhysRevLett.76.4468](https://doi.org/10.1103/PhysRevLett.76.4468). arXiv: [hep-ph/9602226](https://arxiv.org/abs/hep-ph/9602226).
- [42] A. Freitas and P. Schwaller. “Higgs CP Properties From Early LHC Data”. In: *Phys. Rev. D* 87.5 (2013), p. 055014. DOI: [10.1103/PhysRevD.87.055014](https://doi.org/10.1103/PhysRevD.87.055014). arXiv: [1211.1980](https://arxiv.org/abs/1211.1980) [[hep-ph](#)].
- [43] P. Agrawal, S. Mitra, and A. Shivaji. “Effect of Anomalous Couplings on the Associated Production of a Single Top Quark and a Higgs Boson at the LHC”. In: *JHEP* 12 (2013), p. 077. DOI: [10.1007/JHEP12\(2013\)077](https://doi.org/10.1007/JHEP12(2013)077). arXiv: [1211.4362](https://arxiv.org/abs/1211.4362) [[hep-ph](#)].
- [44] A. Djouadi and G. Moreau. “The couplings of the Higgs boson and its CP properties from fits of the signal strengths and their ratios at the 7+8 TeV LHC”. In: *Eur. Phys. J. C* 73.9 (2013), p. 2512. DOI: [10.1140/epjc/s10052-013-2512-9](https://doi.org/10.1140/epjc/s10052-013-2512-9). arXiv: [1303.6591](https://arxiv.org/abs/1303.6591) [[hep-ph](#)].
- [45] J. Ellis et al. “Disentangling Higgs-Top Couplings in Associated Production”. In: *JHEP* 04 (2014), p. 004. DOI: [10.1007/JHEP04\(2014\)004](https://doi.org/10.1007/JHEP04(2014)004). arXiv: [1312.5736](https://arxiv.org/abs/1312.5736) [[hep-ph](#)].
- [46] J. Yue. “Enhanced  $thj$  signal at the LHC with  $h \rightarrow \gamma\gamma$  decay and  $CP$ -violating top-Higgs coupling”. In: *Phys. Lett. B* 744 (2015), pp. 131–136. DOI: [10.1016/j.physletb.2015.03.044](https://doi.org/10.1016/j.physletb.2015.03.044). arXiv: [1410.2701](https://arxiv.org/abs/1410.2701) [[hep-ph](#)].
- [47] F. Demartin et al. “Higgs characterisation at NLO in QCD: CP properties of the top-quark Yukawa interaction”. In: *Eur. Phys. J. C* 74.9 (2014), p. 3065. DOI: [10.1140/epjc/s10052-014-3065-2](https://doi.org/10.1140/epjc/s10052-014-3065-2). arXiv: [1407.5089](https://arxiv.org/abs/1407.5089) [[hep-ph](#)].
- [48] J. Chang et al. “Probing the Top-Yukawa Coupling in Associated Higgs production with a Single Top Quark”. In: *JHEP* 05 (2014), p. 062. DOI: [10.1007/JHEP05\(2014\)062](https://doi.org/10.1007/JHEP05(2014)062). arXiv: [1403.2053](https://arxiv.org/abs/1403.2053) [[hep-ph](#)].
- [49] X.-G. He, G.-N. Li, and Y.-J. Zheng. “Probing Higgs boson  $CP$  Properties with  $t\bar{t}H$  at the LHC and the 100 TeV  $pp$  collider”. In: *Int. J. Mod. Phys. A* 30.25 (2015), p. 1550156. DOI: [10.1142/S0217751X15501560](https://doi.org/10.1142/S0217751X15501560). arXiv: [1501.00012](https://arxiv.org/abs/1501.00012) [[hep-ph](#)].
- [50] F. Demartin et al. “Higgs production in association with a single top quark at the LHC”. In: *Eur. Phys. J. C* 75.6 (2015), p. 267. DOI: [10.1140/epjc/s10052-015-3475-9](https://doi.org/10.1140/epjc/s10052-015-3475-9). arXiv: [1504.00611](https://arxiv.org/abs/1504.00611) [[hep-ph](#)].

- [51] F. Boudjema et al. “Lab-frame observables for probing the top-Higgs interaction”. In: *Phys. Rev. D* 92.1 (2015), p. 015019. DOI: [10.1103/PhysRevD.92.015019](https://doi.org/10.1103/PhysRevD.92.015019). arXiv: [1501.03157](https://arxiv.org/abs/1501.03157) [hep-ph].
- [52] M. R. Buckley and D. Goncalves. “Boosting the Direct CP Measurement of the Higgs-Top Coupling”. In: *Phys. Rev. Lett.* 116.9 (2016), p. 091801. DOI: [10.1103/PhysRevLett.116.091801](https://doi.org/10.1103/PhysRevLett.116.091801). arXiv: [1507.07926](https://arxiv.org/abs/1507.07926) [hep-ph].
- [53] F. Demartin et al. “tWH associated production at the LHC”. In: *Eur. Phys. J. C* 77.1 (2017), p. 34. DOI: [10.1140/epjc/s10052-017-4601-7](https://doi.org/10.1140/epjc/s10052-017-4601-7). arXiv: [1607.05862](https://arxiv.org/abs/1607.05862) [hep-ph].
- [54] A. V. Gritsan et al. “Constraining anomalous Higgs boson couplings to the heavy flavor fermions using matrix element techniques”. In: *Phys. Rev. D* 94.5 (2016), p. 055023. DOI: [10.1103/PhysRevD.94.055023](https://doi.org/10.1103/PhysRevD.94.055023). arXiv: [1606.03107](https://arxiv.org/abs/1606.03107) [hep-ph].
- [55] N. Mileo et al. “Pseudoscalar top-Higgs coupling: exploration of CP-odd observables to resolve the sign ambiguity”. In: *JHEP* 07 (2016), p. 056. DOI: [10.1007/JHEP07\(2016\)056](https://doi.org/10.1007/JHEP07(2016)056). arXiv: [1603.03632](https://arxiv.org/abs/1603.03632) [hep-ph].
- [56] A. Kobakhidze et al. “Implications of CP-violating Top-Higgs Couplings at LHC and Higgs Factories”. In: *Phys. Rev. D* 95.1 (2017), p. 015016. DOI: [10.1103/PhysRevD.95.015016](https://doi.org/10.1103/PhysRevD.95.015016). arXiv: [1610.06676](https://arxiv.org/abs/1610.06676) [hep-ph].
- [57] D. Azevedo et al. “CP tests of Higgs couplings in  $t\bar{t}h$  semileptonic events at the LHC”. In: *Phys. Rev. D* 98.3 (2018), p. 033004. DOI: [10.1103/PhysRevD.98.033004](https://doi.org/10.1103/PhysRevD.98.033004). arXiv: [1711.05292](https://arxiv.org/abs/1711.05292) [hep-ph].
- [58] D. Gonçalves, K. Kong, and J. H. Kim. “Probing the top-Higgs Yukawa CP structure in dileptonic  $t\bar{t}h$  with  $M_2$ -assisted reconstruction”. In: *JHEP* 06 (2018), p. 079. DOI: [10.1007/JHEP06\(2018\)079](https://doi.org/10.1007/JHEP06(2018)079). arXiv: [1804.05874](https://arxiv.org/abs/1804.05874) [hep-ph].
- [59] W.-S. Hou, M. Kohda, and T. Modak. “Probing for extra top Yukawa couplings in light of  $t\bar{t}h(125)$  observation”. In: *Phys. Rev. D* 98.7 (2018), p. 075007. DOI: [10.1103/PhysRevD.98.075007](https://doi.org/10.1103/PhysRevD.98.075007). arXiv: [1806.06018](https://arxiv.org/abs/1806.06018) [hep-ph].
- [60] Q.-H. Cao et al. “Limiting top quark-Higgs boson interaction and Higgs-boson width from multitop productions”. In: *Phys. Rev. D* 99.11 (2019), p. 113003. DOI: [10.1103/PhysRevD.99.113003](https://doi.org/10.1103/PhysRevD.99.113003). arXiv: [1901.04567](https://arxiv.org/abs/1901.04567) [hep-ph].
- [61] D. A. Faroughy et al. “Probing the CP nature of the top quark Yukawa at hadron colliders”. In: *JHEP* 02 (2020), p. 085. DOI: [10.1007/JHEP02\(2020\)085](https://doi.org/10.1007/JHEP02(2020)085). arXiv: [1909.00007](https://arxiv.org/abs/1909.00007) [hep-ph].
- [62] J. Ren, L. Wu, and J. M. Yang. “Unveiling CP property of top-Higgs coupling with graph neural networks at the LHC”. In: *Phys. Lett. B* 802 (2020), p. 135198. DOI: [10.1016/j.physletb.2020.135198](https://doi.org/10.1016/j.physletb.2020.135198). arXiv: [1901.05627](https://arxiv.org/abs/1901.05627) [hep-ph].
- [63] M. Kraus et al. “Exploring BSM Higgs couplings in single top-quark production”. In: (Aug. 2019). arXiv: [1908.09100](https://arxiv.org/abs/1908.09100) [hep-ph].
- [64] B. Bortolato et al. “Optimized probes of CP-odd effects in the  $t\bar{t}h$  process at hadron colliders”. In: *Nucl. Phys. B* 964 (2021), p. 115328. DOI: [10.1016/j.nuclphysb.2021.115328](https://doi.org/10.1016/j.nuclphysb.2021.115328). arXiv: [2006.13110](https://arxiv.org/abs/2006.13110) [hep-ph].

- [65] Q.-H. Cao et al. “A New Observable for Measuring CP Property of Top-Higgs Interaction”. In: *Chin. Phys. C* 45.2 (2021), p. 023117. DOI: [10.1088/1674-1137/abcfac](https://doi.org/10.1088/1674-1137/abcfac). arXiv: [2008.13442](https://arxiv.org/abs/2008.13442) [[hep-ph](#)].
- [66] H. Bahl et al. “Indirect  $\mathcal{CP}$  probes of the Higgs-top-quark interaction: current LHC constraints and future opportunities”. In: *JHEP* 11 (2020), p. 127. DOI: [10.1007/JHEP11\(2020\)127](https://doi.org/10.1007/JHEP11(2020)127). arXiv: [2007.08542](https://arxiv.org/abs/2007.08542) [[hep-ph](#)].
- [67] T. Martini et al. “Probing the CP structure of the top quark Yukawa coupling: Loop sensitivity versus on-shell sensitivity”. In: *Phys. Rev. D* 104.5 (2021), p. 055045. DOI: [10.1103/PhysRevD.104.055045](https://doi.org/10.1103/PhysRevD.104.055045). arXiv: [2104.04277](https://arxiv.org/abs/2104.04277) [[hep-ph](#)].
- [68] R. K. Barman, D. Gonçalves, and F. Kling. “Machine learning the Higgs boson-top quark CP phase”. In: *Phys. Rev. D* 105.3 (2022), p. 035023. DOI: [10.1103/PhysRevD.105.035023](https://doi.org/10.1103/PhysRevD.105.035023). arXiv: [2110.07635](https://arxiv.org/abs/2110.07635) [[hep-ph](#)].
- [69] H. Bahl and S. Brass. “Constraining  $\mathcal{CP}$ -violation in the Higgs-top-quark interaction using machine-learning-based inference”. In: *JHEP* 03 (2022), p. 017. DOI: [10.1007/JHEP03\(2022\)017](https://doi.org/10.1007/JHEP03(2022)017). arXiv: [2110.10177](https://arxiv.org/abs/2110.10177) [[hep-ph](#)].
- [70] D. Gonçalves et al. “Direct Higgs-top CP-phase measurement with  $t\bar{t}h$  at the 14 TeV LHC and 100 TeV FCC”. In: *JHEP* 01 (2022), p. 158. DOI: [10.1007/JHEP01\(2022\)158](https://doi.org/10.1007/JHEP01(2022)158). arXiv: [2108.01083](https://arxiv.org/abs/2108.01083) [[hep-ph](#)].
- [71] D. Azevedo et al. “CP-violation, asymmetries and interferences in  $t\bar{t}\phi$ ”. In: *JHEP* 09 (2022), p. 246. DOI: [10.1007/JHEP09\(2022\)246](https://doi.org/10.1007/JHEP09(2022)246). arXiv: [2208.04271](https://arxiv.org/abs/2208.04271) [[hep-ph](#)].
- [72] A. Butter et al. “Two Invertible Networks for the Matrix Element Method”. In: (Sept. 2022). arXiv: [2210.00019](https://arxiv.org/abs/2210.00019) [[hep-ph](#)].
- [73] J. Ackerschott et al. “Returning CP-Observables to The Frames They Belong”. In: (July 2023). arXiv: [2308.00027](https://arxiv.org/abs/2308.00027) [[hep-ph](#)].
- [74] A. Bhardwaj et al. “Non-linear top-Higgs CP violation”. In: (Aug. 2023). arXiv: [2308.11722](https://arxiv.org/abs/2308.11722) [[hep-ph](#)].
- [75] G. Klamke and D. Zeppenfeld. “Higgs plus two jet production via gluon fusion as a signal at the CERN LHC”. In: *JHEP* 04 (2007), p. 052. DOI: [10.1088/1126-6708/2007/04/052](https://doi.org/10.1088/1126-6708/2007/04/052). arXiv: [hep-ph/0703202](https://arxiv.org/abs/hep-ph/0703202).
- [76] K. Hagiwara, Q. Li, and K. Mawatari. “Jet angular correlation in vector-boson fusion processes at hadron colliders”. In: *JHEP* 07 (2009), p. 101. DOI: [10.1088/1126-6708/2009/07/101](https://doi.org/10.1088/1126-6708/2009/07/101). arXiv: [0905.4314](https://arxiv.org/abs/0905.4314) [[hep-ph](#)].
- [77] C. Englert et al. “Higgs Quantum Numbers in Weak Boson Fusion”. In: *JHEP* 01 (2013), p. 148. DOI: [10.1007/JHEP01\(2013\)148](https://doi.org/10.1007/JHEP01(2013)148). arXiv: [1212.0843](https://arxiv.org/abs/1212.0843) [[hep-ph](#)].
- [78] C. Englert et al. “Approaching robust EFT limits for CP-violation in the Higgs sector”. In: *Phys. Rev. D* 99.9 (2019), p. 095007. DOI: [10.1103/PhysRevD.99.095007](https://doi.org/10.1103/PhysRevD.99.095007). arXiv: [1901.05982](https://arxiv.org/abs/1901.05982) [[hep-ph](#)].
- [79] Z. Yu, K. A. Mohan, and C.-P. Yuan. “Determining the CP Property of  $ht\bar{t}$  Coupling via a Novel Jet Substructure Observable”. In: (Nov. 2022). arXiv: [2211.00845](https://arxiv.org/abs/2211.00845) [[hep-ph](#)].



- [80] ATLAS Collaboration. <https://atlas.web.cern.ch/Atlas/GROUPS/PHYSICS/PUBNOTES/ATL-PHYS-PUB-2023-025/>. 2023.
- [81] CMS Collaboration. <https://twiki.cern.ch/twiki/bin/view/CMSPublic/PhysicsResultsSUS>. 2023.
- [82] ATLAS Collaboration. <https://atlas.web.cern.ch/Atlas/GROUPS/PHYSICS/PUBNOTES/ATL-PHYS-PUB-2023-018/>. 2023.
- [83] ATLAS Collaboration. <https://atlas.web.cern.ch/Atlas/GROUPS/PHYSICS/PUBNOTES/ATL-PHYS-PUB-2023-006/>. 2023.
- [84] ATLAS Collaboration. <https://atlas.web.cern.ch/Atlas/GROUPS/PHYSICS/PUBNOTES/ATL-PHYS-PUB-2022-007/>. 2023.
- [85] CMS Collaboration. <https://twiki.cern.ch/twiki/bin/view/CMSPublic/SummaryPlotsEX013TeV>. 2023.
- [86] D. de Florian et al. “Handbook of LHC Higgs Cross Sections: 4. Deciphering the Nature of the Higgs Sector”. In: 2/2017 (Oct. 2016). DOI: [10.23731/CYRM-2017-002](https://doi.org/10.23731/CYRM-2017-002). arXiv: [1610.07922](https://arxiv.org/abs/1610.07922) [[hep-ph](#)].
- [87] J. R. Andersen et al. “Loop induced interference effects in Higgs Boson plus two jet production at the LHC”. In: *JHEP* 02 (2008), p. 057. DOI: [10.1088/1126-6708/2008/02/057](https://doi.org/10.1088/1126-6708/2008/02/057). arXiv: [0709.3513](https://arxiv.org/abs/0709.3513) [[hep-ph](#)].
- [88] A. Bredenstein, K. Hagiwara, and B. Jager. “Mixed QCD-electroweak contributions to Higgs-plus-dijet production at the LHC”. In: *Phys. Rev. D* 77 (2008), p. 073004. DOI: [10.1103/PhysRevD.77.073004](https://doi.org/10.1103/PhysRevD.77.073004). arXiv: [0801.4231](https://arxiv.org/abs/0801.4231) [[hep-ph](#)].
- [89] P. Artoisenet et al. “A framework for Higgs characterisation”. In: *JHEP* 11 (2013), p. 043. DOI: [10.1007/JHEP11\(2013\)043](https://doi.org/10.1007/JHEP11(2013)043). arXiv: [1306.6464](https://arxiv.org/abs/1306.6464) [[hep-ph](#)].
- [90] A. Dedes et al. “Feynman rules for the Standard Model Effective Field Theory in  $R_\xi$  - gauges”. In: *JHEP* 06 (), p. 143. DOI: [10.1007/JHEP06\(2017\)143](https://doi.org/10.1007/JHEP06(2017)143). arXiv: [1704.03888](https://arxiv.org/abs/1704.03888) [[hep-ph](#)].
- [91] G. Aad et al. “Measurement of the properties of Higgs boson production at  $\sqrt{s} = 13$  TeV in the  $H \rightarrow \gamma\gamma$  channel using  $139 \text{ fb}^{-1}$  of  $pp$  collision data with the ATLAS experiment”. In: *JHEP* 07 (2023), p. 088. DOI: [10.1007/JHEP07\(2023\)088](https://doi.org/10.1007/JHEP07(2023)088). arXiv: [2207.00348](https://arxiv.org/abs/2207.00348) [[hep-ex](#)].
- [92] J. Alwall et al. “The automated computation of tree-level and next-to-leading order differential cross sections, and their matching to parton shower simulations”. In: *Journal of High Energy Physics* 2014.7 (July 2014). DOI: [10.1007/jhep07\(2014\)079](https://doi.org/10.1007/jhep07(2014)079). URL: <https://doi.org/10.1007%2Fjhep07%282014%29079>.
- [93] T. Sjostrand, S. Mrenna, and P. Z. Skands. “A Brief Introduction to PYTHIA 8.1”. In: *Comput. Phys. Commun.* 178 (2008), pp. 852–867. DOI: [10.1016/j.cpc.2008.01.036](https://doi.org/10.1016/j.cpc.2008.01.036). arXiv: [0710.3820](https://arxiv.org/abs/0710.3820) [[hep-ph](#)].
- [94] J. de Favereau et al. “DELPHES 3: a modular framework for fast simulation of a generic collider experiment”. In: *Journal of High Energy Physics* 2014.2 (Feb. 2014). DOI: [10.1007/jhep02\(2014\)057](https://doi.org/10.1007/jhep02(2014)057). URL: <https://doi.org/10.1007%2Fjhep02%282014%29057>.

- [95] M. Cacciari, G. P. Salam, and G. Soyez. “The anti- $k_t$  jet clustering algorithm”. In: *JHEP* 04 (2008), p. 063. DOI: [10.1088/1126-6708/2008/04/063](https://doi.org/10.1088/1126-6708/2008/04/063). arXiv: [0802.1189](https://arxiv.org/abs/0802.1189) [[hep-ph](#)].
- [96] C. Degrande et al. “UFO - The Universal FeynRules Output”. In: *Comput. Phys. Commun.* 183 (2012), pp. 1201–1214. DOI: [10.1016/j.cpc.2012.01.022](https://doi.org/10.1016/j.cpc.2012.01.022). arXiv: [1108.2040](https://arxiv.org/abs/1108.2040) [[hep-ph](#)].
- [97] L. Darmé et al. “UFO 2.0: the ‘Universal Feynman Output’ format”. In: *Eur. Phys. J. C* 83.7 (2023), p. 631. DOI: [10.1140/epjc/s10052-023-11780-9](https://doi.org/10.1140/epjc/s10052-023-11780-9). arXiv: [2304.09883](https://arxiv.org/abs/2304.09883) [[hep-ph](#)].
- [98] M. Buschmann et al. “Resolving the Higgs-Gluon Coupling with Jets”. In: *Phys. Rev. D* 90.1 (2014), p. 013010. DOI: [10.1103/PhysRevD.90.013010](https://doi.org/10.1103/PhysRevD.90.013010). arXiv: [1405.7651](https://arxiv.org/abs/1405.7651) [[hep-ph](#)].
- [99] F. Maltoni, E. Vryonidou, and M. Zaro. “Top-quark mass effects in double and triple Higgs production in gluon-gluon fusion at NLO”. In: *JHEP* 11 (2014), p. 079. DOI: [10.1007/JHEP11\(2014\)079](https://doi.org/10.1007/JHEP11(2014)079). arXiv: [1408.6542](https://arxiv.org/abs/1408.6542) [[hep-ph](#)].
- [100] X. Chen et al. “Top-quark mass effects in H+jet and H+2 jets production”. In: *JHEP* 03 (2022), p. 096. DOI: [10.1007/JHEP03\(2022\)096](https://doi.org/10.1007/JHEP03(2022)096). arXiv: [2110.06953](https://arxiv.org/abs/2110.06953) [[hep-ph](#)].
- [101] F. Pedregosa et al. “Scikit-learn: Machine Learning in Python”. In: *Journal of Machine Learning Research* 12 (2011), pp. 2825–2830.
- [102] A. Bhardwaj et al. “Machine-enhanced CP-asymmetries in the Higgs sector”. In: *Phys. Lett. B* 832 (2022), p. 137246. DOI: [10.1016/j.physletb.2022.137246](https://doi.org/10.1016/j.physletb.2022.137246). arXiv: [2112.05052](https://arxiv.org/abs/2112.05052) [[hep-ph](#)].
- [103] S. M. Lundberg and S.-I. Lee. “A Unified Approach to Interpreting Model Predictions”. In: *Advances in Neural Information Processing Systems 30*. Ed. by I. Guyon et al. Curran Associates, Inc., 2017, pp. 4765–4774. URL: <http://papers.nips.cc/paper/7062-a-unified-approach-to-interpreting-model-predictions.pdf>.
- [104] G. Owen. *Game Theory*. Academic Press, 1982.
- [105] R. B. Myerson. *Game Theory: Analysis of Conflict*. Harvard University Press, 1997.
- [106] E. Štrumbelj and I. Kononenko. “An Efficient Explanation of Individual Classifications using Game Theory”. In: *Journal of Machine Learning Research* 11.1 (2010), pp. 1–18. URL: <http://jmlr.org/papers/v11/strumbelj10a.html>.
- [107] A. Butter et al. “Back to the Formula – LHC Edition”. In: (Sept. 2021). arXiv: [2109.10414](https://arxiv.org/abs/2109.10414) [[hep-ph](#)].
- [108] P. Bechtle et al. “*HiggsSignals*: Confronting arbitrary Higgs sectors with measurements at the Tevatron and the LHC”. In: *Eur. Phys. J. C* 74.2 (2014), p. 2711. DOI: [10.1140/epjc/s10052-013-2711-4](https://doi.org/10.1140/epjc/s10052-013-2711-4). arXiv: [1305.1933](https://arxiv.org/abs/1305.1933) [[hep-ph](#)].
- [109] P. Bechtle et al. “*HiggsSignals-2*: Probing new physics with precision Higgs measurements in the LHC 13 TeV era”. In: *Eur. Phys. J. C* 81.2 (2021), p. 145. DOI: [10.1140/epjc/s10052-021-08942-y](https://doi.org/10.1140/epjc/s10052-021-08942-y). arXiv: [2012.09197](https://arxiv.org/abs/2012.09197) [[hep-ph](#)].

- [110] H. Bahl et al. “HiggsTools: BSM scalar phenomenology with new versions of HiggsBounds and HiggsSignals”. In: *Comput. Phys. Commun.* 291 (2023), p. 108803. DOI: [10.1016/j.cpc.2023.108803](https://doi.org/10.1016/j.cpc.2023.108803). arXiv: [2210.09332](https://arxiv.org/abs/2210.09332) [[hep-ph](#)].
- [111] G. Aad et al. “Measurement of Higgs boson decay into  $b$ -quarks in associated production with a top-quark pair in  $pp$  collisions at  $\sqrt{s} = 13$  TeV with the ATLAS detector”. In: *JHEP* 06 (2022), p. 097. DOI: [10.1007/JHEP06\(2022\)097](https://doi.org/10.1007/JHEP06(2022)097). arXiv: [2111.06712](https://arxiv.org/abs/2111.06712) [[hep-ex](#)].
- [112] V. M. Abazov et al. “A precision measurement of the mass of the top quark”. In: *Nature* 429 (2004), pp. 638–642. DOI: [10.1038/nature02589](https://doi.org/10.1038/nature02589). arXiv: [hep-ex/0406031](https://arxiv.org/abs/hep-ex/0406031).
- [113] Y. Gao et al. “Spin Determination of Single-Produced Resonances at Hadron Colliders”. In: *Phys. Rev. D* 81 (2010), p. 075022. DOI: [10.1103/PhysRevD.81.075022](https://doi.org/10.1103/PhysRevD.81.075022). arXiv: [1001.3396](https://arxiv.org/abs/1001.3396) [[hep-ph](#)].
- [114] J. Alwall, A. Freitas, and O. Mattelaer. “The Matrix Element Method and QCD Radiation”. In: *Phys. Rev. D* 83 (2011), p. 074010. DOI: [10.1103/PhysRevD.83.074010](https://doi.org/10.1103/PhysRevD.83.074010). arXiv: [1010.2263](https://arxiv.org/abs/1010.2263) [[hep-ph](#)].
- [115] S. Bolognesi et al. “On the spin and parity of a single-produced resonance at the LHC”. In: *Phys. Rev. D* 86 (2012), p. 095031. DOI: [10.1103/PhysRevD.86.095031](https://doi.org/10.1103/PhysRevD.86.095031). arXiv: [1208.4018](https://arxiv.org/abs/1208.4018) [[hep-ph](#)].
- [116] P. Avery et al. “Precision studies of the Higgs boson decay channel  $H \rightarrow ZZ \rightarrow 4\ell$  with MEKD”. In: *Phys. Rev. D* 87.5 (2013), p. 055006. DOI: [10.1103/PhysRevD.87.055006](https://doi.org/10.1103/PhysRevD.87.055006). arXiv: [1210.0896](https://arxiv.org/abs/1210.0896) [[hep-ph](#)].
- [117] J. R. Andersen, C. Englert, and M. Spannowsky. “Extracting precise Higgs couplings by using the matrix element method”. In: *Phys. Rev. D* 87.1 (2013), p. 015019. DOI: [10.1103/PhysRevD.87.015019](https://doi.org/10.1103/PhysRevD.87.015019). arXiv: [1211.3011](https://arxiv.org/abs/1211.3011) [[hep-ph](#)].
- [118] P. Artoisenet et al. “Unravelling  $t\bar{t}h$  via the Matrix Element Method”. In: *Phys. Rev. Lett.* 111.9 (2013), p. 091802. DOI: [10.1103/PhysRevLett.111.091802](https://doi.org/10.1103/PhysRevLett.111.091802). arXiv: [1304.6414](https://arxiv.org/abs/1304.6414) [[hep-ph](#)].
- [119] J. M. Campbell et al. “Finding the Higgs Boson in Decays to  $Z\gamma$  using the Matrix Element Method at Next-to-Leading Order”. In: *Phys. Rev. D* 87.7 (2013), p. 073005. DOI: [10.1103/PhysRevD.87.073005](https://doi.org/10.1103/PhysRevD.87.073005). arXiv: [1301.7086](https://arxiv.org/abs/1301.7086) [[hep-ph](#)].
- [120] T. Martini and P. Uwer. “The Matrix Element Method at next-to-leading order QCD for hadronic collisions: Single top-quark production at the LHC as an example application”. In: *JHEP* 05 (2018), p. 141. DOI: [10.1007/JHEP05\(2018\)141](https://doi.org/10.1007/JHEP05(2018)141). arXiv: [1712.04527](https://arxiv.org/abs/1712.04527) [[hep-ph](#)].
- [121] J. Brehmer et al. “Mining gold from implicit models to improve likelihood-free inference”. In: *Proc. Nat. Acad. Sci.* 117.10 (2020), pp. 5242–5249. DOI: [10.1073/pnas.1915980117](https://doi.org/10.1073/pnas.1915980117). arXiv: [1805.12244](https://arxiv.org/abs/1805.12244) [[stat.ML](#)].
- [122] J. Brehmer et al. “Constraining Effective Field Theories with Machine Learning”. In: *Phys. Rev. Lett.* 121.11 (2018), p. 111801. DOI: [10.1103/PhysRevLett.121.111801](https://doi.org/10.1103/PhysRevLett.121.111801). arXiv: [1805.00013](https://arxiv.org/abs/1805.00013) [[hep-ph](#)].



- [123] J. Brehmer et al. “A Guide to Constraining Effective Field Theories with Machine Learning”. In: *Phys. Rev. D* 98.5 (2018), p. 052004. DOI: [10.1103/PhysRevD.98.052004](https://doi.org/10.1103/PhysRevD.98.052004). arXiv: [1805.00020](https://arxiv.org/abs/1805.00020) [[hep-ph](#)].
- [124] M. Stoye et al. “Likelihood-free inference with an improved cross-entropy estimator”. In: (Aug. 2018). arXiv: [1808.00973](https://arxiv.org/abs/1808.00973) [[stat.ML](#)].
- [125] J. Brehmer et al. “MadMiner: Machine learning-based inference for particle physics”. In: *Comput. Softw. Big Sci.* 4.1 (2020), p. 3. DOI: [10.1007/s41781-020-0035-2](https://doi.org/10.1007/s41781-020-0035-2). arXiv: [1907.10621](https://arxiv.org/abs/1907.10621) [[hep-ph](#)].
- [126] I. Brivio. “SMEFTsim 3.0 — a practical guide”. In: *JHEP* 04 (2021), p. 073. DOI: [10.1007/JHEP04\(2021\)073](https://doi.org/10.1007/JHEP04(2021)073). arXiv: [2012.11343](https://arxiv.org/abs/2012.11343) [[hep-ph](#)].
- [127] S. S. Wilks. “The Large-Sample Distribution of the Likelihood Ratio for Testing Composite Hypotheses”. In: *The Annals of Mathematical Statistics* 9.1 (1938), pp. 60–62. DOI: [10.1214/aoms/1177732360](https://doi.org/10.1214/aoms/1177732360). URL: <https://doi.org/10.1214/aoms/1177732360>.